WL-TR-91-2064

A SURVEY OF OPTICAL DIAGNOSTIC METHODS FOR THE STUDY OF FUEL FOULING

T. E. Parker
R. R. Foutter
W. T. Rawlins

Physical Sciences Inc.
20 New England Business Center
Andover, MA 01810

June 1991

Final Report for Period July 1990 - January 1991

AERO PROPULSION & POWER DIRECTORATE
WRIGHT LABORATORY
AIR FORCE SYSTEMS COMMAND
WRIGHT-PATTERSON AIR FORCE BASE, OHIO 45433-6563

NOTICE

When Government drawings, specifications, or other data are used for any purpose other than in connection with a definitely Government-related procurement, the United States Government incurs no responsibility nor any obligation whatsoever. The fact that the government may have formulated, or in any way supplied the said drawings, specifications, or other data, is not to be regarded by implication or otherwise in any manner construed, as licensing the holder or any other person or corporation, or as conveying any rights or permission to manufacture, use, or sell any patented invention that may in any way be related thereto.

This report is releasable to the National Technical Information Service (NTIS). At NTIS, it will be available to the general public, including foreign nations.

This technical report has been reviewed and is approved for publication.

JEFFREY A. PEARCE, Capt, USAF
Fuels Branch
Fuels and Lubrication Division
Aero Propulsion and Power Directorate

CHARLES L. DELANEY, Chief
Fuels Branch
Fuels and Lubrication Division
Aero Propulsion and Power Directorate

FOR THE COMMANDER

LEO S. HAROOTYAN, Chief
Fuels and Lubrication Division
Aero Propulsion and Power Directorate

If your address has changed, if you wish to be removed from our mailing list, or if the addressee is no longer employed by your organization, please notify WL/POSF, Wright-Patterson AFB, OH 45433-6563 to help us maintain a current mailing list.

Copies of this report should not be returned unless return is required by security considerations, contractual obligations, or notice on a specific document.

REPORT DOCUMENTATION PAGE

1a. REPORT SECURITY CLASSIFICATION UNCLASSIFIED	1b. RESTRICTIVE MARKINGS N/A
2a. SECURITY CLASSIFICATION AUTHORITY	3 DISTRIBUTION / AVAILABILITY OF REPORT Approved for public release; distribution is unlimited.
2b. DECLASSIFICATION / DOWNGRADING SCHEDULE	
4. PERFORMING ORGANIZATION REPORT NUMBER(S) PSI-2143/TR-1115	5. MONITORING ORGANIZATION REPORT NUMBER(S) WL-TR-91-2064
6a. NAME OF PERFORMING ORGANIZATION Physical Sciences Inc. 6b. OFFICE SYMBOL (If applicable)	7a. NAME OF MONITORING ORGANIZATION Aero Propulsion & Power Dir. (WL/POSF) Wright Laboratory
6c. ADDRESS (City, State, and ZIP Code) 20 New England Business Center Andover, MA 01810	7b. ADDRESS (City, State, and ZIP Code) Wright Patterson Air Force Base Ohio 45433-6563
8a. NAME OF FUNDING / SPONSORING ORGANIZATION Aero Propulsion & Power Dir. 8b. OFFICE SYMBOL (If applicable) WL/POSF	9. PROCUREMENT INSTRUMENT IDENTIFICATION NUMBER F33615-90-C-2068
8c. ADDRESS (City, State, and ZIP Code) Wright-Patterson Air Force Base Ohio 45433-6563	10. SOURCE OF FUNDING NUMBERS PROGRAM ELEMENT NO. 65502F; PROJECT NO. 3005; TASK NO. 21; WORK UNIT ACCESSION NO 91

11. TITLE (Include Security Classification)

A Survey of Optical Diagnostic Methods for the Study of Fuel Fouling

12. PERSONAL AUTHOR(S) T.E. Parker, R.R., Foutter, and W.T. Rawlins

13a. TYPE OF REPORT	13b. TIME COVERED	14. DATE OF REPORT (Year, Month, Day)	15. PAGE COUNT
Final	FROM 7/31/90 TO 1/31/91	June 1991	49

16. SUPPLEMENTARY NOTATION

17. COSATI CODES			18. SUBJECT TERMS (Continue on reverse if necessary and identify by block number)
FIELD	GROUP	SUB-GROUP	Optical diagnostics, scattering, fluorescence, absorption, fuel fouling

19. ABSTRACT (Continue on reverse if necessary and identify by block number)

An experimental study of fuel fouling using optical measurement methods was performed. These measurements included absorption from 350 to 750 nm, scattering at 514.5 nm, and fluorescence using a probe wavelength of 514.5 nm. Measurements were performed using a constant temperature heating system which exited into an optical cell. Each of the measurements proved useful in monitoring changes in the test fuel, JP-4, at test temperatures up to 775 K and pressures of 400 psig. Absorption measurements at temperatures between ambient and 860 K indicated dramatic changes in the thermally stressed fuel. These changes included indications of both molecular changes in the fuel composition and a dramatic increase in the particulate present in the flow. Relative kinetic behavior for the absorption measurement indicated that both temperature and residence time were controlling variables in the fouling process. Arrhenius plots of the absorption results illustrated that the fouling behavior could be grouped into two constant slope regions with a transition region near 525 K. Scattering measurements indicated room temperature fuel to contain

20. DISTRIBUTION / AVAILABILITY OF ABSTRACT ☐ UNCLASSIFIED/UNLIMITED ☐ SAME AS RPT ☒ DTIC USERS	21 ABSTRACT SECURITY CLASSIFICATION UNCLASSIFIED
22a. NAME OF RESPONSIBLE INDIVIDUAL Capt Jeffrey A. Pearce	22b. TELEPHONE (Include Area Code) (513) 255-4160 22c. OFFICE SYMBOL WL/POSF

DD FORM 1473, 84 MAR 83 APR edition may be used until exhausted.
All other editions are obsolete.

particulate with average diameters greater than 0.1 μm while thermally stressed fuel contained much larger concentrations of particulate with sizes below 0.06 μm. Fluorescence signal intensities behaved, over the experimental temperature range in a manner similar to scattering intensities and displayed significant variations in spectral structure with temperature. This work clearly illustrates the possibilities of using optical methods for monitoring the fuel fouling process.

TABLE OF CONTENTS

LIST OF FIGURES

LIST OF FIGURES (Continued)

1. INTRODUCTION

Hydrocarbon fuels, such as those used in aircraft propulsion systems, degrade when exposed to high temperature environments and create surface deposits which can dramatically change both the heat transfer characteristics and mechanical tolerances of critical assemblies. The surface deposition process, known as fouling, is a poorly understood phenomenon dependent upon many parameters such as fuel composition, oxygen content, impurities, such as metals and sulfur compounds, temperature, exposure time, surface composition, and surface morphology. The development of fuels and fuel systems for extreme temperature service in high performance engines requires a better understanding of the fouling process. A logical step to develop this understanding is the application of optical diagnostics, developed for the study of combustion processes, to the fuel fouling problem. This paper reports initial results for absorption, scattering, and fluorescence measurements that have been used to monitor the changes in a thermally stressed fuel.

The degradation of fuels in storage tanks and high temperature systems has been an engineering problem for many decades and a wealth of literature is available on the subject. A brief review of some of this literature is included in the following paragraphs. In 1989, Roquemore[1] et al. proposed that a greater fundamental understanding of fuel fouling was necessary because of the increased fuel operating temperatures for future aircraft. This understanding would come in part by applying existing optical measurement techniques to the fuel fouling problem. In fact, an optical method was developed for monitoring fuel stability in diesel storage tanks as early as 1955.[2] The fouling process has very notably been studied by Taylor and co-workers.[3-7] Results from these works include quantifying the role of oxygen in the deposition process and starting to define importance of trace sulfur compounds for deposition processes. In addition, these works identified the existence of three temperature regimes for deposition with oxygen bearing fuels. Fuel composition effects were also examined by monitoring deposition with paraffins and paraffin/aromatic mixes. Other investigations have shown that deposition rates may be enhanced by the presence of

deposits.[8] Optical absorption was used by Kendall and Mills[9] to quantify the role of trace species, iron, and copper. These workers also confirmed that fuel stability could be enhanced by removing oxygen and sulfur and using a metal deactivating additive to reduce catalytic effects from trace copper and iron in the fuel.[10] This sample of the literature indicates that fuel fouling is a complex process which can be affected by temperature, oxygen contact, molecular fuel contact, trace compounds (such as sulfur, copper, and iron), and the presence of deposits.

2. EXPERIMENTAL DESCRIPTION

The experimental setup for this work is most simply discussed in two parts: the fuel handling and heating apparatus and the optical configurations used to monitor absorption, scattering, and fluorescence of the fuel. The fuel used for this study was a JP-4 manufactured and analyzed by Phillips petroleum and the fuel was used in its as-received condition. The dissolved gas (nitrogen and oxygen) in the fuel was not quantified. Results of a fuel analysis are included in Table 1.

A schematic diagram for the fuel handling and heating hardware is shown in Figure 1. The fuel is stored and pressurized in a 0.25 gallon steel reservoir fitted with a neoprene bladder. The bladder is filled with nitrogen which is used to keep the fuel at a constant 400 psig pressure. A section of 0.25 in. diameter stainless tubing is used to connect the fuel reservoir to a 0.375 in. tube which is imbedded in a heated copper block. This 0.375 in. tube is 55 in. in length, and connects to a an optical cell manufactured from 316 stainless steel.

The interior dimension for the cell is 1 in. square by 3 in. long, and four 0.75 in. diameter optical ports for quartz windows are included at directions orthogonal to the flow. The windows which were used for the absorption measurements were manufactured from 1.25 in. diameter, 0.5 in. thick quartz; these windows were modified to include a 0.25 in.

Table 1. Fuel Analysis of JP-4 Used in This Study

Test	Results	MIL-T-5624 Specifications
API Gravity	56.2	45.0 → 57.0
Corrosion	1A	1B Max.
Total Sulfur	0.09	0.4 Max.
Doctor Test	Negative	Negative
Smoke Point	36.0	20 Min.
Freeze Point	< -58	-58 Max.
Aniline Point	122	Report
Aniline Gravity Product	6,856	5,250
Total Acidity	0.005	0.015
Color (Saybolt)	+30	Report
Existent Gums	0.2	7 Max.
Hydrogen Content (wt%)	14.4	13.6
Conductivity	203	200 → 600
WSIM	85	70 Min.
RVP	2.3	2 → 3
Particulates (mg/l)	0.03	1 Max.
Water Reaction Interface	1B	1B
Filtration Time (min)	4	10 Max.
Distillation, D-86, °C		
IBP	76	Report
10	86	Report
20	89	145 Max.
50	101	190 Max.
90	193	245 Max.
95	205	Report
EP	216	270 Max.
Loss	0.4	1.5 Max.
Residue	1.0	1.5 Max.
Hydrocarbon Type, Vol. %		
Aromatics	9.9	25 Max.
Olefins	0.0	5 Max.
Saturated	90.1	Remainder
	100.0	
JFTOT P (mmHg)	0.0	25 Max.
JFTOT Tube Color Test	1	<3
Anti-Icing	0.11	0.1 → 0.15
Antioxidant	Added	Required
Antistatic	Added	Required

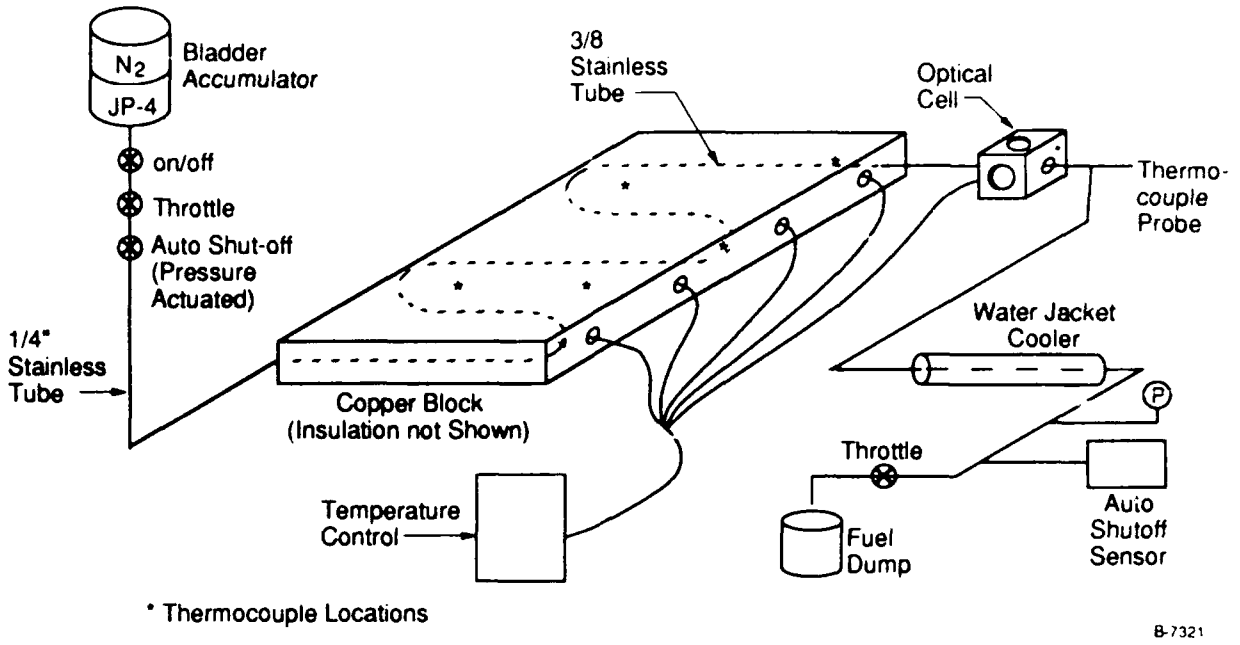

Figure 1. Schematic Diagram of the Fuel - Fouling Apparatus

deep step to allow the windows to be flush with the cell wall. Scattering and fluorescence measurements used windows which had no steps and therefore were not flush with the cell wall. Both the cell and windows were designed to operate at elevated temperatures (up to 900 K) and pressures (up to 750 psi). A major factor in the design and construction of the cell was the seal between the quartz and the stainless steel. The difficulty with this type of seal is that the two materials have dramatically different thermal expansion coefficients. Given a temperature range from ambient to 900 K, a certain amount of relative motion between the two materials is inevitable. The solution for this system was a spiral wound gasket made of alternate layers of stainless steel and carbon fiber (manufactured under the trade name Grafoil Stainless Steel and manufactured by Atlantic Gasket Company). As an added precaution, a layer of carbon cloth was used between the window holders (used to press the windows into the gaskets) and the window.

After exiting from the cell, the fuel is cooled in a water jacketed heat exchanger and emptied into a fuel dump. Fuel flow rate is controlled with a throttling valve located

immediately after the heat exchanger and monitored simply with a graduated cylinder and a stop watch. An automatic shutoff system is also included in the experimental setup to minimize the hazards associated with a window failure. The system monitors pressure at the exit of the fuel cooler. In the event of a sudden loss of pressure, a valve upstream of the copper block is automatically closed.

The test rig which has just been described is designed to thermally stress the fuel in a very controlled manner. The fuel is heated as it flows through the tube in the copper block and the bulk fuel temperature asymptotically approaches the block temperature. Temperature variations within the block are insignificant due to its thickness (1.25 in.) and the high thermal conductivity of the copper. A variety of thermocouple temperature measurements were included in the experiment and they verified that the copper block acted as a constant temperature reservoir within a 10 percent tolerance range. The bulk fuel temperature for this constant wall temperature system is given by Eq. (1):[11]

$$\frac{T_o - T_m}{T_o - T_e} = \exp\left[\frac{-k\ N_u}{r^2 \rho c_p}\right] \frac{x}{u} \qquad (1)$$

$T_{o,m,e}$ - temperature at the surface, bulk fluid, and fluid at the entrance of the heater
k - thermal conductivity
Nu - Nusselt number for the flow
r - tube radius
ρ - fuel density
c_p - specific heat of the fuel
x - distance from the entrance
u - mean flow velocity

This solution does not include thermal entry length effects but due to the low Reynolds number they were determined to be insignificant. Figure 2 illustrates the temperature profile for the bulk fuel temperature and also illustrates the effect of flow rate on the residence time within the system. As shown by Figure 2, the rig is capable of subjecting the fuel to a known temperature (the temperature of the copper block) for a known period of time.

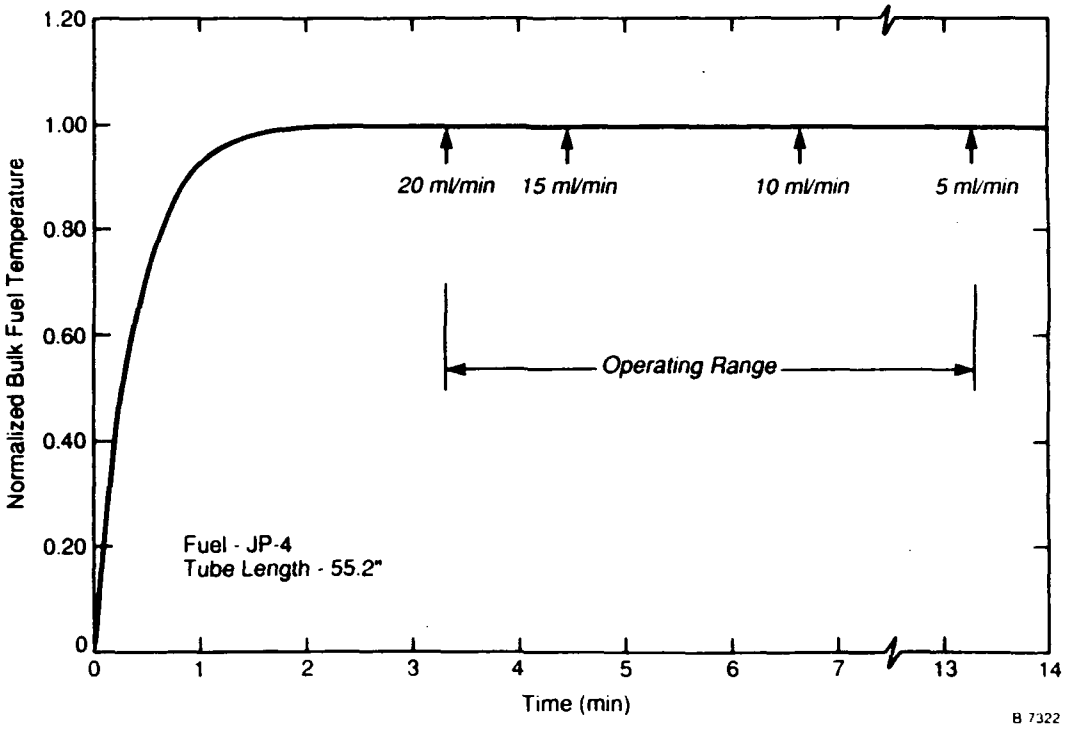

Figure 2. Thermal History of the Bulk Temperature for the Fuel as it Flows Through the Apparatus. Residence times are controlled with the volumetric flow rate of the fuel

The temperature of the fuel as it exits the optical cell was also monitored closely since the cell was heated separately from the copper block. A decrease in the temperature of the optical cell from that of the copper block will drive the temperature of the fuel down. For the absorption measurements, this effect was observed to depress the temperature of the fuel by approximately 10 percent. However, for the scattering and fluorescence measurements, the cell heater was not operational, and the temperature of the fuel in the cell was observed to drop by up to 40 percent from the temperature of the copper block. Although this deviates from the ideal constant temperature experiment which one hopes to perform, the results remain valid with the understanding that a small fraction of the thermal history of the fuel does not follow the profile shown in Figure 2.

The optical measurements were done in two series with distinct optical setups; one for absorption and the other for scattering and fluorescence. The absorption setup is shown in Figure 3. A tungsten-halogen light powered with a regulated d.c. supply (Oriel model

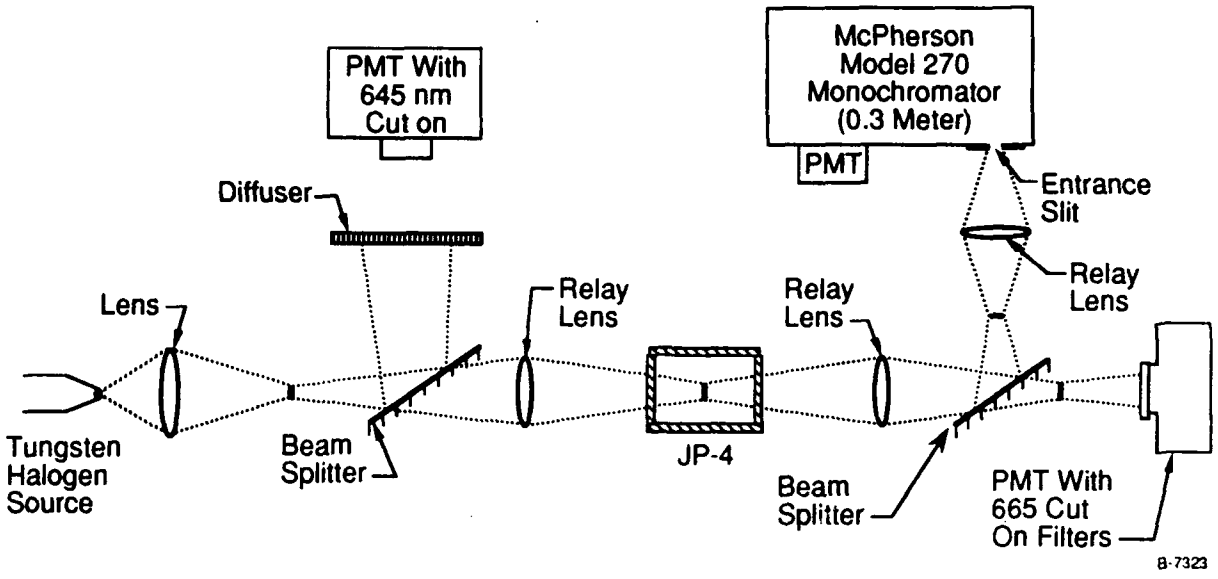

Figure 3. Schematic Diagram of the Optical Setup for Measuring the Absorption Properties of the Fuel

#68735) was used as the broadband source. Relay lenses were used to image the source in the center of the cell and the lens to image light path was confined to a diameter significantly smaller than the clear aperture of the windows. A quartz flat was used as a partial beam splitter before the cell to direct a fraction of the light onto a filtered photo-multiplier tube used as a power monitor. A neutral density filter (optical density 1.0) was used in a similar fashion after the cell to direct the light into both a filtered photomultiplier tube and a 0.35 meter monochromator. The monochromator was set to scan from 350 to 750 nm and included a 360 nm cut on filter to minimize second order signal between 700 and 750 nm and to provide an accurate zero level signal for the scan. Second order signals were verified to constitute less than 0.1 percent of the signal between 700 and 750 nm. Wavelength resolution for this system (1200 groove/mm grating, 100 μm slits, and 4 mm slit height) was approximately 0.3 nm. Signals from the three photomultiplier tubes were digitized using a Data Translation DT2801(A) interfaced to an IBM PC. The scanning rate for the monochromator was 200 nm/min, data acquisition was 15 Hz, and the frequency response for each of the photomultiplier tubes was approximately 500 Hz. This setup could then be used

in a convenient fashion to monitor the absorption of the fuel in the cell as a function of wavelength. Data analysis from this measurement is described later in this paper.

A different optical configuration was used to monitor the scattering and fluorescence from the thermally stressed fuel in the cell as shown in Figure 4. In this configuration a beam from an Ar^+ laser (514.5 nm) is directed through the cell and the collection paths for scattering and fluorescence are placed at right angles to the beam. The beam is chopped at approximately 20 Hz before it enters the cell and laser power is monitored using a quartz flat as a beam splitter and photomultiplier tube with a notch filter. The optics for monitoring the scattering from particulate in the fuel are carefully arranged to minimize the effects of scattering from both the interior of the cell and the external beam path. A pair of 400 mm focal length lenses were used with the focus of the collection lens placed in the center of the cell and the focus from the second lens placed on a pinhole used as a limiting aperture for the photomultiplier tube. The two lenses were separated by 240 mm and a baffle between the lens pair was adjusted to a diameter of 10 mm. This optical train very effectively

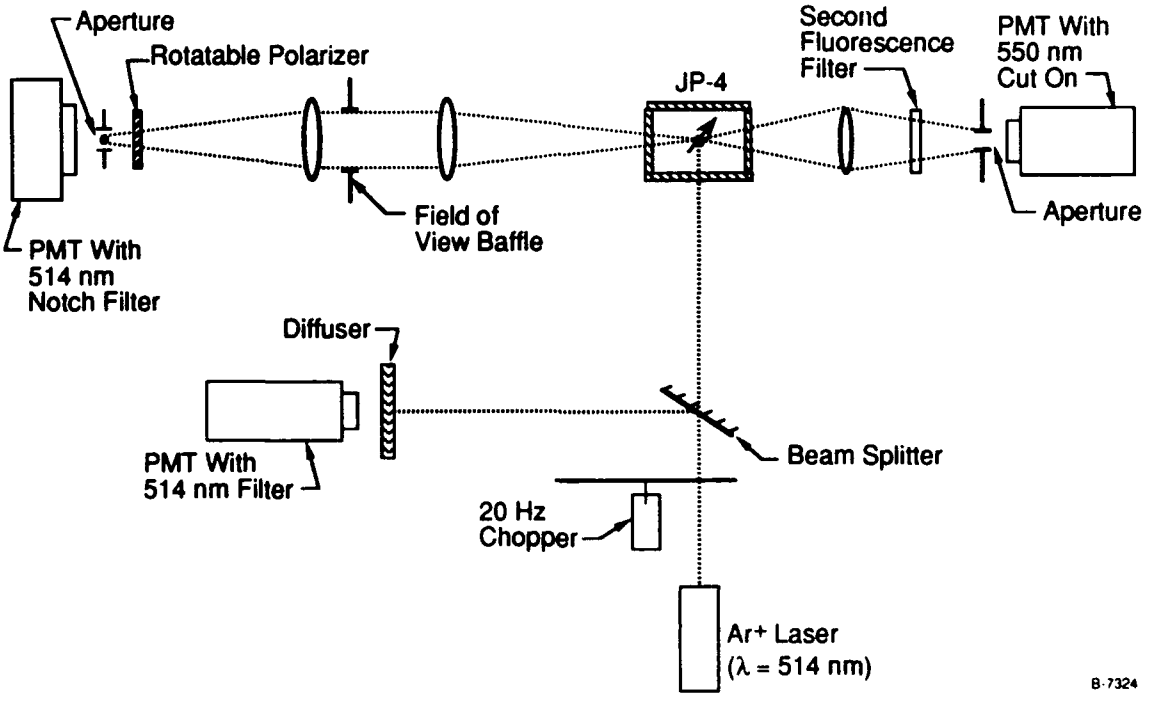

Figure 4. Schematic Diagram for Scattering and Fluorescence in the Fuel Cell

confined the field of view to the quartz windows on either side cell. As a test of the effectiveness of this setup, the signal levels for the system were checked with no fuel in the cell. This test verifies that contributions from randomly scattered light were less than 0.1 percent of the signals observed in the scattering experiments.

The scattering optical train included a rotatable polarizer located in front of the photomultiplier tube. This polarizer could be positioned to admit light polarized perpendicular or parallel to the plane defined by the laser beam and the detector. The polarization of the laser was carefully controlled to include a 50 percent component in each of these directions. This setup could then be used to monitor scattering from both perpendicular and parallel states.

The optical train for collecting the fluorescence signal used the window opposite that used for scattering and utilized a single lens imaging system to direct the light from the center of the cell to an aperture in front of the photomultiplier. A 550 nm long pass filter was used to exclude the probe wavelength (514.5 nm) and provision for a second filter was incorporated into the optical path. Successive use of a series of filters with different cut on wavelengths allowed crude determination of the fluorescence spectrum.

3. RESULTS

Using the experimental apparatus just described, absorption, scattering, and fluorescence were monitored for fuel that was subjected to temperatures up to 750 K at pressures of 400 psi. The following discussion treats the absorption results first, followed by an analysis of scattering and fluorescence data.

The absorption measurement is quite simply a record of the spectral character of the transmissive properties of the fuel, and the motivation for a large spectral range of data is to use the variation in absorption with wavelength to characterize the absorbing species in the

fuel. The measurements which are reported have been normalized for variations in the lamp's power output and the post cell photomultiplier signal was in all cases examined for significant variations during a monochromator scan. The apparatus was operated in steady state fashion and therefore the absorption signal from the post-cell PMT should be (and was) constant. Equation (2) defines the observed transmission, defined as the ratio of light intensity after traversing the cell to that entering the cell. The loss in intensity can be attributed to reflection losses at the quartz/air interface, losses at the quartz/fuel interface, and the extinction/absorption observed for the optical path length through fuel. Equation (2) neglects secondary reflections from the optical interfaces. For these experiments the reflectivity at the quartz/fuel interface is effectively zero as shown by inspection of Eq. (3); the real index of refraction for quartz varies from 1.477 to 1.455[12] over the 350 to 750 nm range. The index of refraction for JP-4 can be inferred by examining the indices of refraction for the normal alkanes (decane through tetradecane) which have indices in the visible between 1.41 and 1.43[13] and toluene whose index is 1.49.[13] Clearly the difference in refractive index between the fuel and the quartz is small and the energy loss at this interface is inconsequential. Using Eq. (3), the energy loss at the quartz/air interface may also be calculated. The reported absorption results have been adjusted to remove this energy loss and therefore represent absorption within the fuel cell only, Eq. (4). Finally, the absorption results are reported as the negative natural log of the transmission; Eq. (5) reveals that this is simply the summation of the product of number density and optical cross section for the various absorbers in the system.

$$\tau = I/I_0 \approx (1 - R_Q)^2 (1 - R_F)^2 \exp(-\Sigma N_i \sigma_i \ell) \qquad (2)$$

τ	-	transmission
I, I_0	-	light intensity after and before passage through the cell
R_Q	-	reflectance of the quartz/air interface
R_F	-	reflectance of the quartz/fuel interface
N_i	-	number density for component i
σ_i	-	absorption or extinction cross section for component i
ℓ	-	path length in the cell

$$R = \left(\frac{n_2 - n_1}{n_2 + n_1} \right) \tag{3}$$

R - reflectance at the interface
$n_{2,1}$ - real refractive index for the materials bounding the reflecting interface

$$\tau' = \exp(-\Sigma N_i \sigma_i \ell) \tag{4}$$

τ' - transmission for JP-4 only

$$\ln I_0'/I = -\ln\tau' = \Sigma N_i \sigma_i \ell \tag{5}$$

I_0' - beam intensity adjusted for reflectance losses

An example of a transmission curve for the fuel only is shown in Figure 5 for JP-4 in its as-received condition. No significant absorption was observed beyond 500 nm. As a check of the optical integrity of our setup and the data processing we have compared the transmission data for fuel in the optical cell to results using a commercial spectrophotometer (Shimadzu Model UV3100) which have been adjusted for the difference in path length and the energy loss associated with the quartz/air interface. Clearly the agreement is quite good which supports our view that the absorption measurements accurately reflect the properties of the fuel in the cell.

Finally, absorption results assume that deposition on the windows has a negligible effect on transmission during the testing period. This supposition was verified by purging the cell with nitrogen after a test series and comparing the transmission through the cell with that observed before the tests. In all cases; the transmission of the windows was unaffected by window deposits. The reported absorption measurements are therefore a measure of the transmission at the fuel in the cell.

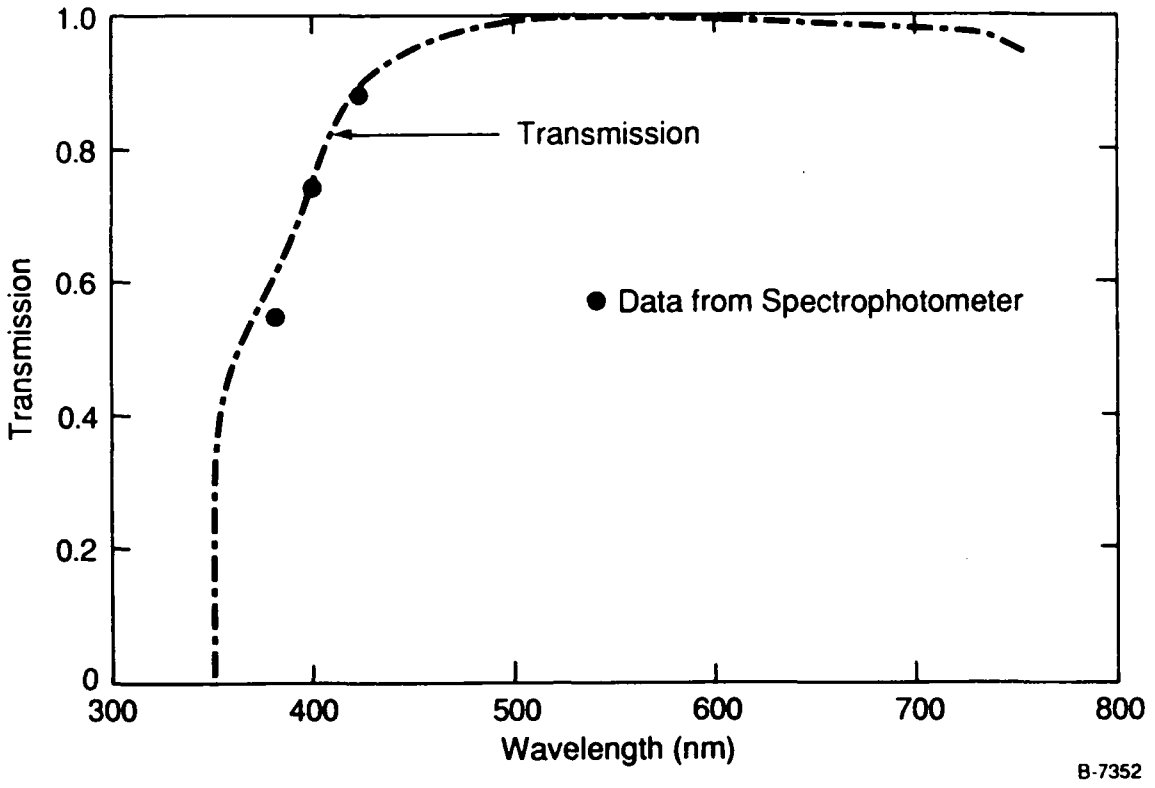

Figure 5. Comparison of the Transmission for JP-4 at Ambient Temperature Using the Absorption Measurement System for the Fuel Cell and a Commercial Spectrophotometer. The transmission measurements are for a 25 mm path length and no losses from window interfaces

Typical low temperature results are shown in Figure 6. The quoted temperature for each of the curves is the temperature of the copper block during the experiment and fuel residence times are approximately 5 min. As previously illustrated by Eq. (5), this plot shows the spectral variation of the product of number density and optical cross section for this system. Comparison of the lowest temperature curve with transmission results for JP-4 which has not been thermally stressed shows no effective change in the absorption properties of the fuel. The fuel is very strongly absorbing in the 400 nm and below region and is essentially transparent beyond 500 nm. This behavior is typical of molecular species which display a very structured absorption spectrum. Particulate on the other hand will act as a broadband absorber and, if present in significant quantity, produce absorption throughout the wavelength range. We therefore primarily attribute the absorption below 500 nm for the low temperature case in Figure 6 to the molecular components of the fuel.

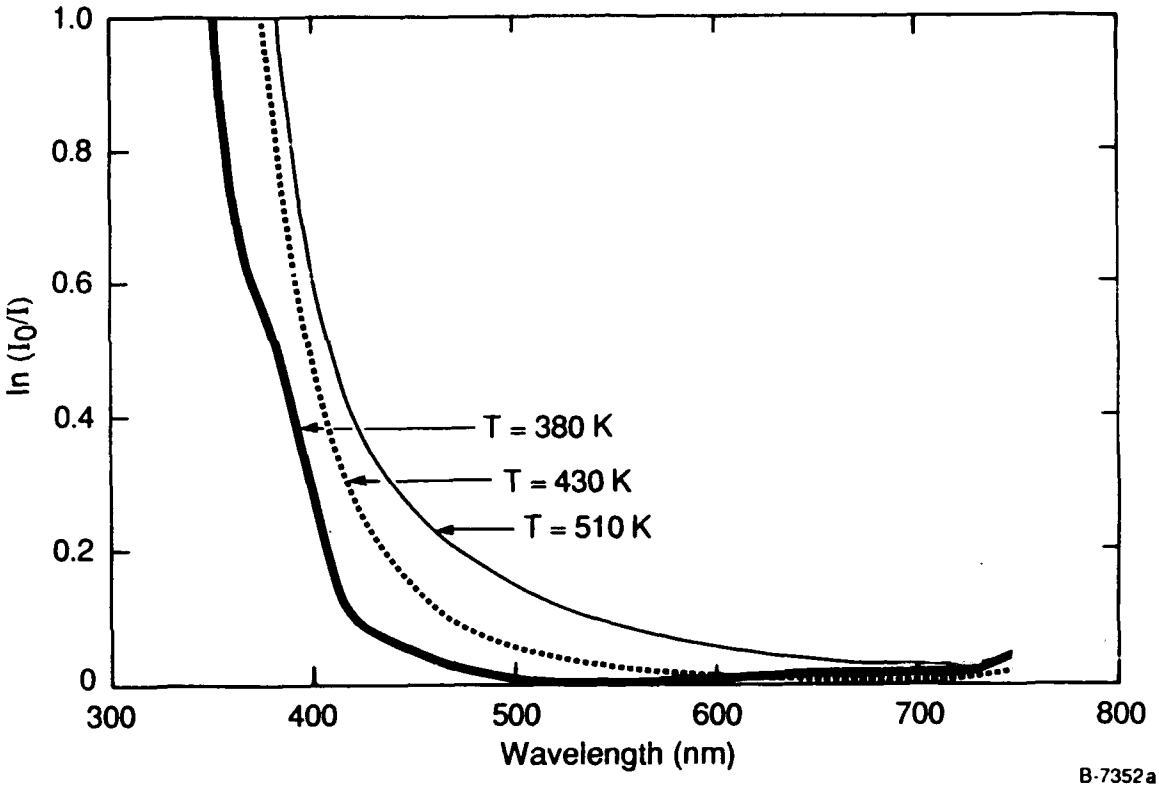

Figure 6. Absorption Characteristics at Three Temperatures for JP-4. The low temperature curve is identical to JP-4 that has not been thermally stressed

Two other absorption spectra are also included in Figure 6 and a comparison of these spectra with the absorption spectra for the unaltered JP-4 (the T=380 K case) is exceptionally interesting. For fuel stressed at 430 K, as in the T=380 K case, the absorption appears to be dominated by molecular absorption. However, the absorption features for this case have been shifted to the red in comparison to the T=380 K result. This shift is indicative of changes in the molecular absorbers for the system. Clearly the concentration or strength of 400 to 500 nm absorbers changed dramatically between the two cases. Temperature effects on the absorption spectra, for this change of temperatures, simply are not large enough to explain the differences in the observed spectra. The wavelength shift associated with a 700 K temperature change is approximately 500 wave-numbers which corresponds to a shift of approximately 2 nm. This shift is clearly insignificant compared to those which are observed.[14] As a final verification of this result, post-thermal-stress absorption scans using a spectrophotometer indicated similar differences in the pre- and post-stressed fuel.

Figure 6 also includes results for fuel which has been processed at 510 K. This result includes significant absorption in the long wavelength regions and the spectral variation is gradual enough to be due, in part, to particulate. However, the absorption behavior below 500 nm is similar to that for the two other temperatures and is primarily due to molecular absorption. Once again, an increased temperature has shifted the absorption further into the red indicating further changes in the molecular components of the fuel. These indicated changes in the fuel's molecular components are not surprising since other studies have shown that fuel deposition on heated surfaces is influenced by the system's chemistry.[3-7] The increasing absorption at long wavelengths is generally an indicator of the presence of compounds with larger molecular structures. For both ring and chain like carbon compounds, increasing the number of rings or atoms in the chain typically increases molecular absorption at longer wavelengths.[15] From a fundamental perspective this is not surprising since increasing the size of the compound increases the number of available electronic states; the energy differences between these states and the ground state becomes smaller and absorption at longer wavelengths becomes possible.[16]

Figure 7 includes results for higher fuel temperatures along with the 380 K result which is included for comparative purposes. Residence times for the 580 K and 600 K results are 5.8 and 4.7 min respectively. Each of the two high temperature results display a broadband absorption signature at the longer wavelengths that is indicative of small size carbon particulate. To illustrate this point, Figure 6 also includes a prediction for particulate absorption assuming Rayleigh limit sizes (diameter $<= 0.01\ \mu m$)[17] using the complex index of refraction for soot.[18] This prediction gives the optical cross section as a function of wavelength; since the absorption measurement gives a product of number density and optical cross section, comparison of the predicted cross section with the measured absorption signal requires the curves to be tied at one point in the spectrum. For this comparison the tie point was 750 nm. Agreement between the absorption signal and the predicted optical cross section as a function of wavelength is excellent.

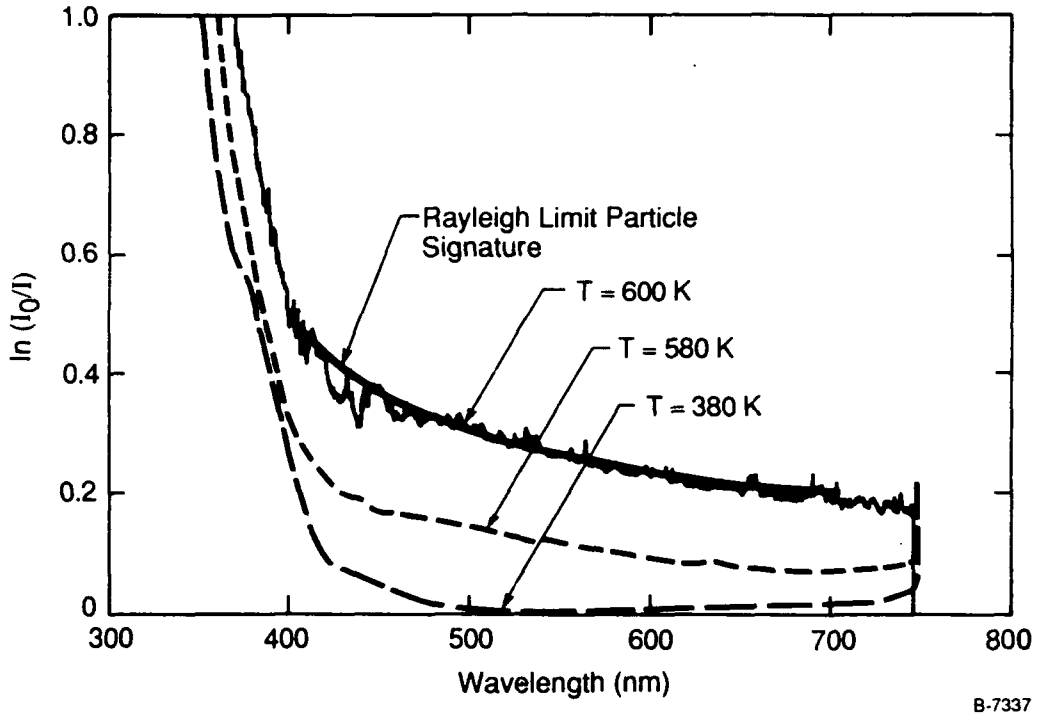

Figure 7. High Temperature Absorption Results for JP-4. An analytical prediction for the absorption characteristics of small particulate is included for comparison with the 600 K result

Figure 8 illustrates an extreme temperature absorption measurement. Residence time for this result was poorly controlled but was estimated to be 7 min. The observed opacity is quite high and for wavelengths longer than 450 nm approximately constant. This constant cross section result is typical for particles that are large with respect to the wavelength.[17]

In order to characterize the optical changes in the fuel due to thermal stress, the baseline absorption signal may be subtracted from that observed at higher temperatures, Eq. (6). These changes are clearly due to the thermal stress on the fuel and, as with other temperature dependent chemical processes, may be presented in an Arrhenius format.

$$\Delta(\Sigma\, N_i\, \sigma_i\, \ell)_{\lambda,T} = (\Sigma\, N_i\, \sigma_i\, \ell)_{\lambda,T} - (\Sigma\, N_i\, \sigma_i\, \ell)_{\lambda,300\ K} \qquad (6)$$

$\Delta(\Sigma\, N_i\, \sigma_i\, \ell)_{\lambda,T}$ - change in the absorption cross sections and number densities of the fuel system. Stressed at temperature T for wavelength λ

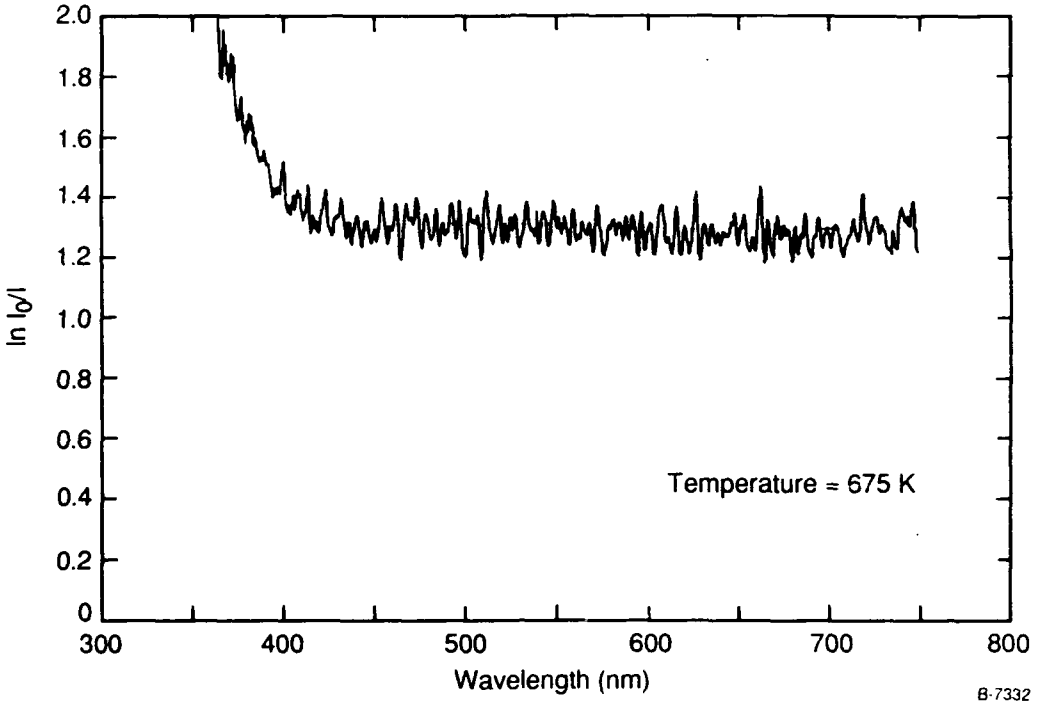

Figure 8. Absorption Results for JP-4 Thermally Stressed at 675 K

Figure 9 illustrates the change in absorption properties of the fuel as a function of temperature for three wavelengths: 400, 550, and 700 nm. Residence times for these results are 4.5 $\pm$ 1.5 min with the exception of two values. Residence times for the data at 700 K and 510 K are 7 and 15 min, respectively. From the previous discussion regarding the spectral nature of the absorption signal, we expect the short wavelength absorption to be indicative of molecular changes in the fuel and the long wavelength absorption to primarily be due to formation of particulate. The results in Figure 9 indicate that substantial amounts of particulate are not formed at temperatures below 510 K. Results for 550 and 400 nm display a complex temperature dependence with the change in absorption increasing with temperature through 510 K, decreasing dramatically over the next 25 deg, and then increasing again with a higher slope. This behavior is exceptionally interesting from the perspective that it implies the disappearance of molecular absorbers between 510 and 525 K and the implication is that these absorbers are consumed at higher temperatures or, conversely, never formed. The dual slope type of result is very similar to that observed in other studies which examined the deposition rate as a function of temperature in heated

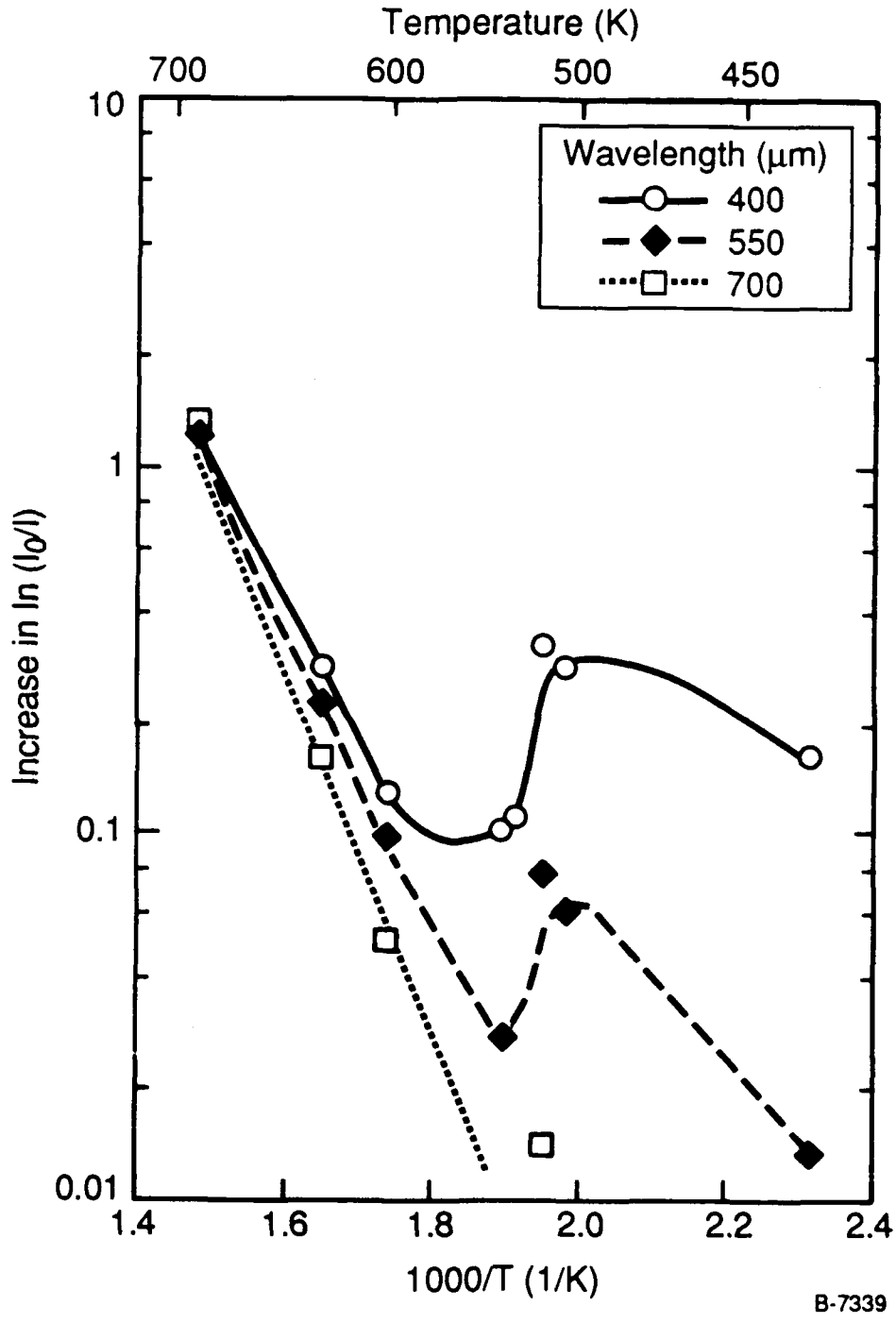

Figure 9. Increase in Optical Absorption due to Temperature. Results are for 400, 550, and 700 nm

stainless tubes.[6] However, the break point between the low and high temperature behavior for this work was approximately 650 K which is significantly higher than the 525 K break point observed optically. Any further comparison between these results is difficult due to the differences in the measurements, the fuels which were used, residence time effects, and oxygen content for the fuel.

Figure 10 is an Arrhenius plot of the ultra-violet absorption data at 375, 400, and 425 nm; residence times are as previously described for Figure 9. Once again this plot displays a dual slope curve with a transition region near 510 K. However, these results display a change in the relative absorption behavior between low and high temperatures. At low temperatures shorter wavelengths absorb more strongly. This behavior, as previously discussed, is typical of molecular absorbers. At the higher temperatures, the difference in absorption with wavelength is not as large and is possibly due to absorption from both particulate and molecules.

Figures 11 and 12 indicate the observed effect of residence time on the increase in optical absorption. Figure 11 illustrates results for fuel exposed to 420 K for 7.6 and 15.2 min. The results, for wavelengths between 400 and 600 nm, are as expected. Prolonged temperature exposure increased the measured absorption. However at 525 K, which is in the transition region shown in Figures 9 and 10, the effect of residence time (3.8 and 5.8 min) is much more interesting. At 600 nm the increased residence time results in a factor of 6 increase in the absorption. However, for shorter wavelengths the increased residence time causes smaller and smaller increases in absorption until, at 400 nm, longer residence time produces less optical absorption. The 400 nm data is exceptionally important since it is a direct indication of the destruction of molecular absorbers with increased exposure time. The implication is that a portion of the 400 nm absorption signal is due to a molecular intermediate which is formed in significant quantity and then consumed as the fuel's chemical makeup evolves.

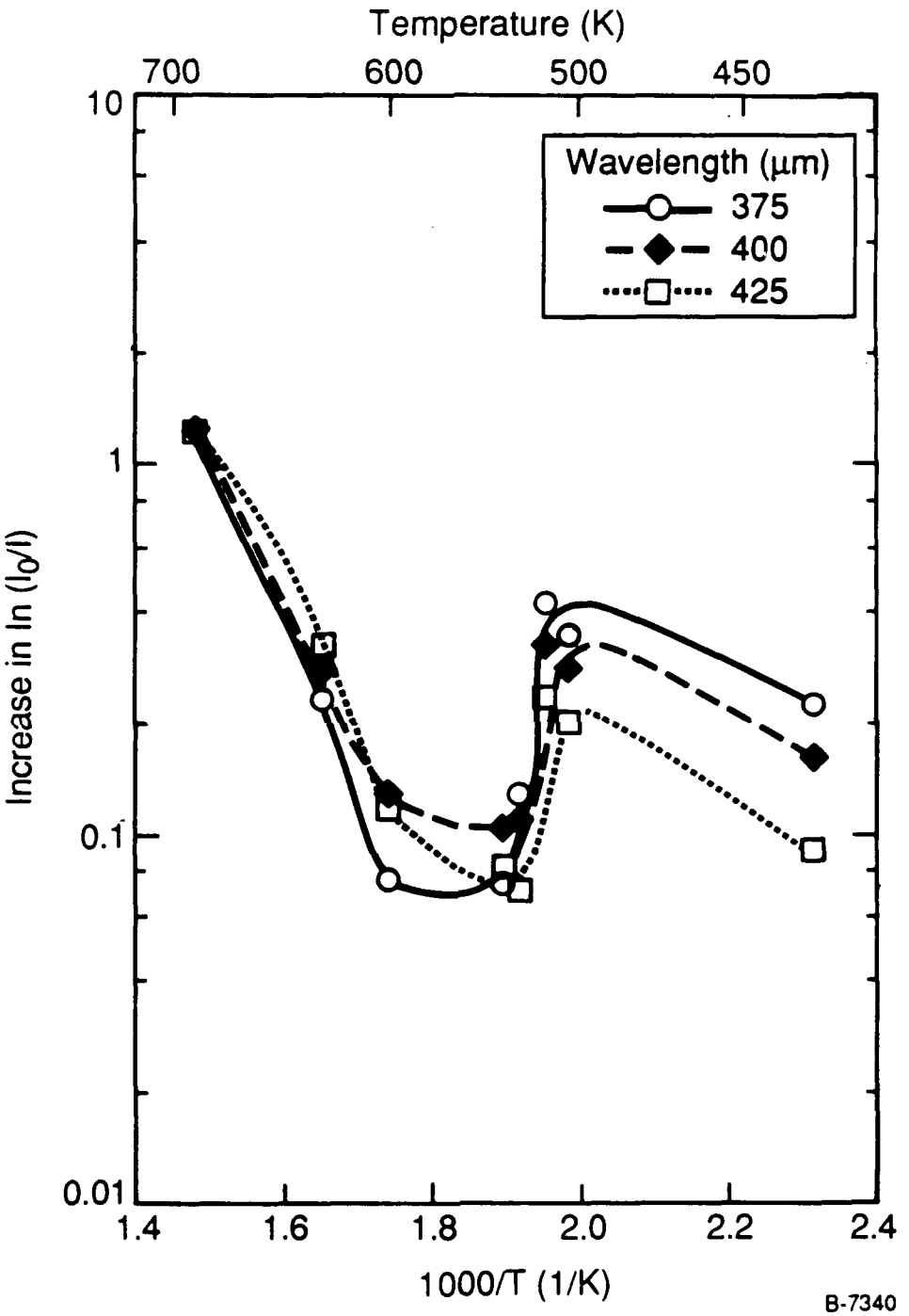

Figure 10. Increase in Optical Absorption due to Temperature. Results are for 375, 400, and 425 nm

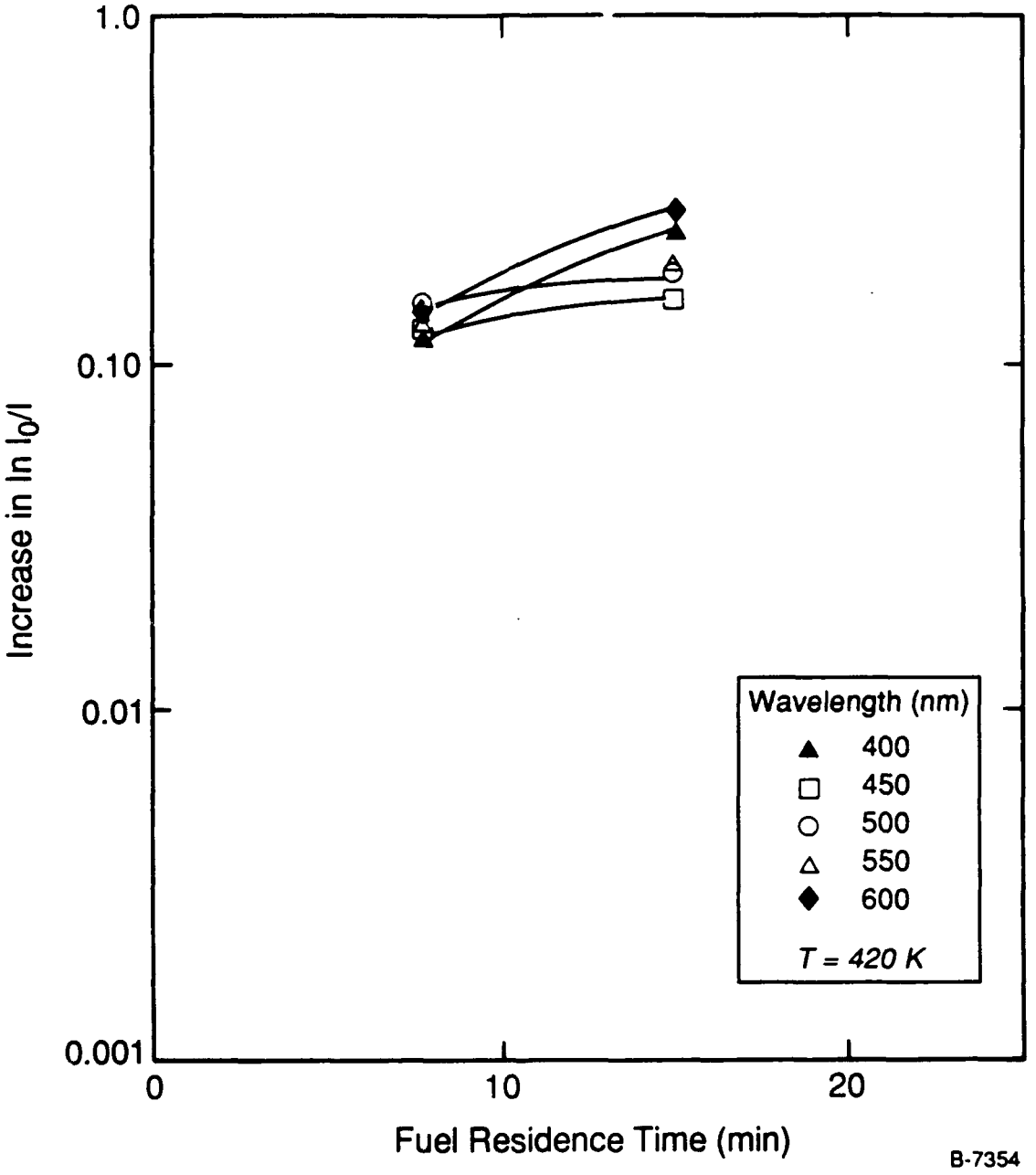

Figure 11. Residence Time Effects on the Change in Optical Absorption for a Low Thermal Stress Temperature

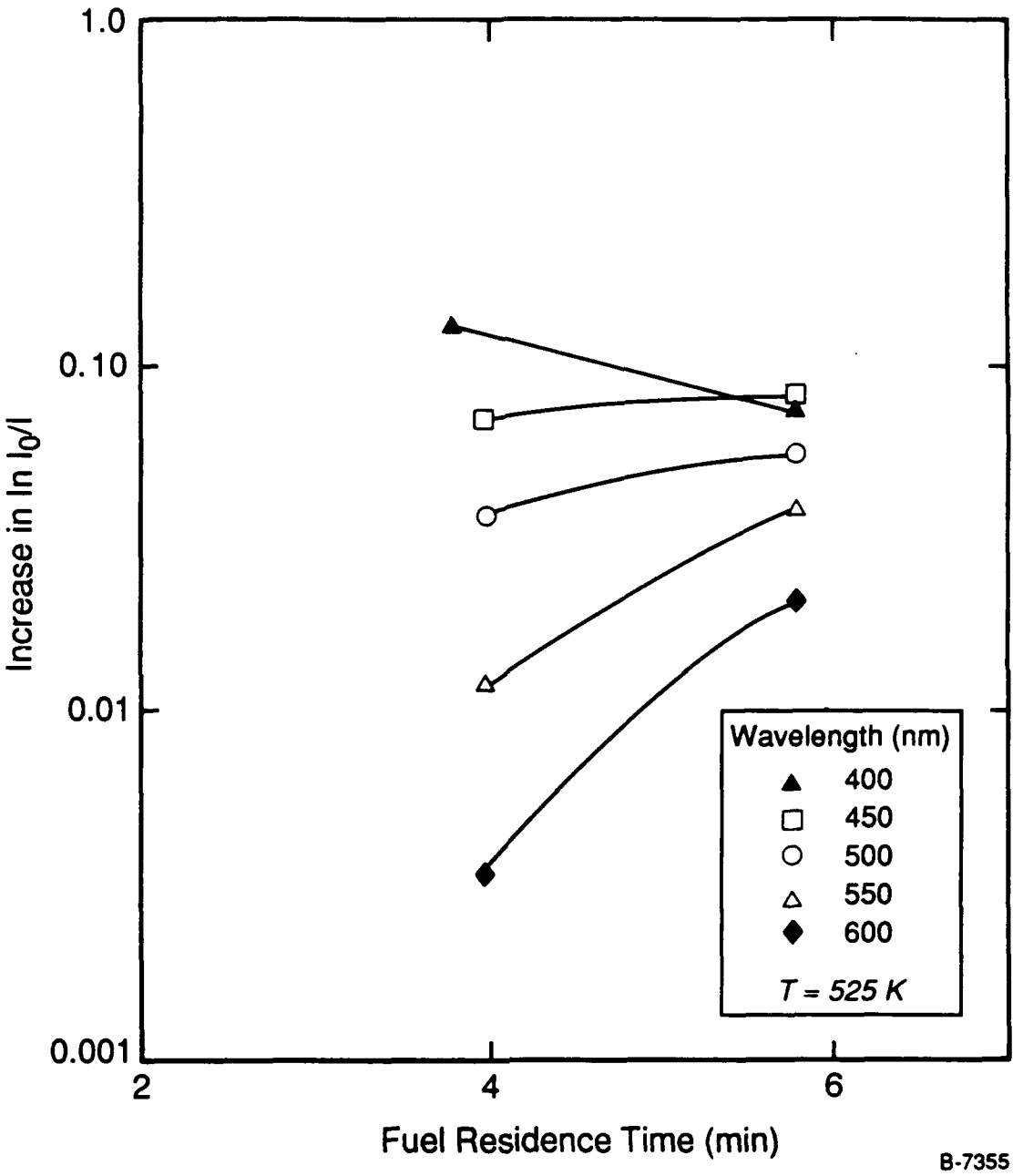

Figure 12. Residence Time Effects on the Change in Optical Absorption for a Moderate Thermal Stress Temperature. The fuel temperature lies in the transition region between low and high temperature behavior observed in Figures 9 and 10

In addition to the absorption results, scattering and fluorescence measurements were made using the optical setup described in Figure 4. The focus for the scattering results was to quantify the size of particulate. Equation (7) gives the relationship between scattering signal and the system parameters. As shown by Eq. (8), the ratio of scattering signal for perpendicular and parallel polarized light is independent of particulate number density and optical probe volume and reduces to a ratio of the scattering cross sections.

$$S = kI_\lambda \, N \, V \, \sigma_s \, \Omega_c \tag{7}$$

S	-	scattering signal
k	-	detector calibration (conversion of incident energy to signal)
N	-	number density of scatterers
σ_s	-	scattering cross section at 90 deg, in cm^2/sterradian
Ω_c	-	optics collection angle
V	-	probe volume

$$\frac{S_\perp}{S_\parallel} = \frac{\sigma_{s,\perp}}{\sigma_{s,\parallel}} \tag{8}$$

$S_{\perp,\parallel}$	-	scattering signal for perpendicular and parallel polarized light
$\sigma_{s,\perp}$, $\sigma_{s,\parallel}$	-	scattering cross section at 90 deg for perpendicular and parallel polarized light

The polarization state for the probe laser was carefully oriented to include an equal component in the planes perpendicular and parallel to the plane defined by the laser propagation and the detection optics. A polarizer in the detection optics could therefore be used to choose either a perpendicular or parallel polarized scattering signal. The ratio of scattering cross sections for orthogonal planes is an established method for monitoring particulate size[17,19] and may be predicted with the mie scattering relationships. Controlling variables for the optical response are the size parameter, defined as the particle circumference divided by the wavelength of the light in the medium, and the ratio of the complex index of refraction of the particulate to that of the medium. Predictions for this

optical cross section ratio are given in Figure 13 and were calculating using indices of refraction typical of carbon particulate (soot).[18] The prediction in Figure 13 also assumes a 5 deg uncertainty in the alignment of the detection system polarizer. This uncertainty is included as an estimate of the accuracy of the system alignment and is the controlling factor in setting the small particle signal ratio.

Figure 13 clearly illustrates that for a monodisperse system, particulate sizing using polarization scattering signal ratioing at a single wavelength can be used to separate the particulate into two size classes: small (for this case less than 0.06 μm radii) and large (greater than 0.06 μm radii). A more definitive particle sizing measurement would require both more accurate alignment of the polarizer and multiple probe wavelengths. Results from the scattering experiments are given in Figure 14 which display the scattering signal ratio in an Arrhenius format. At room temperature, the signal ratio is approximately 3 which indicates that the particulate size is 0.1 μm or greater. Uncertainties in the index of refraction for the particulate make further quantification in the size, given this signal ratio, inappropriate. The change in scattering signal ratio between room temperature fuel and thermally stressed fuel (temperatures greater than 500 K) is dramatic. Clearly the average size has changed distinctly and comparison with the sizing curve included in Figure 13 shows that the particulate has changed from being greater than 0.1 μm at room temperature to being less than 0.06 μm for elevated temperatures. Residence times are in all cases 5 min. This result is exceptionally important from the standpoint that it indicates that the particulate that has been observed for both the absorption and scattering measurements is small in size and present in much higher concentrations than observed in the non-stressed fuel. An estimate in the change in number density may be made by noting that the scattering signal increased by up to 2.5 decades for the thermally stressed fuel while the indicated size moved from greater than 0.1 μm to less than 0.06 μm in radius. The scattering cross section is a function of the sixth power of radius and scattering signal is a function of the number density times the scattering cross section. Therefore, the number density must increase over the room temperature case by a factor of approximately 5000.

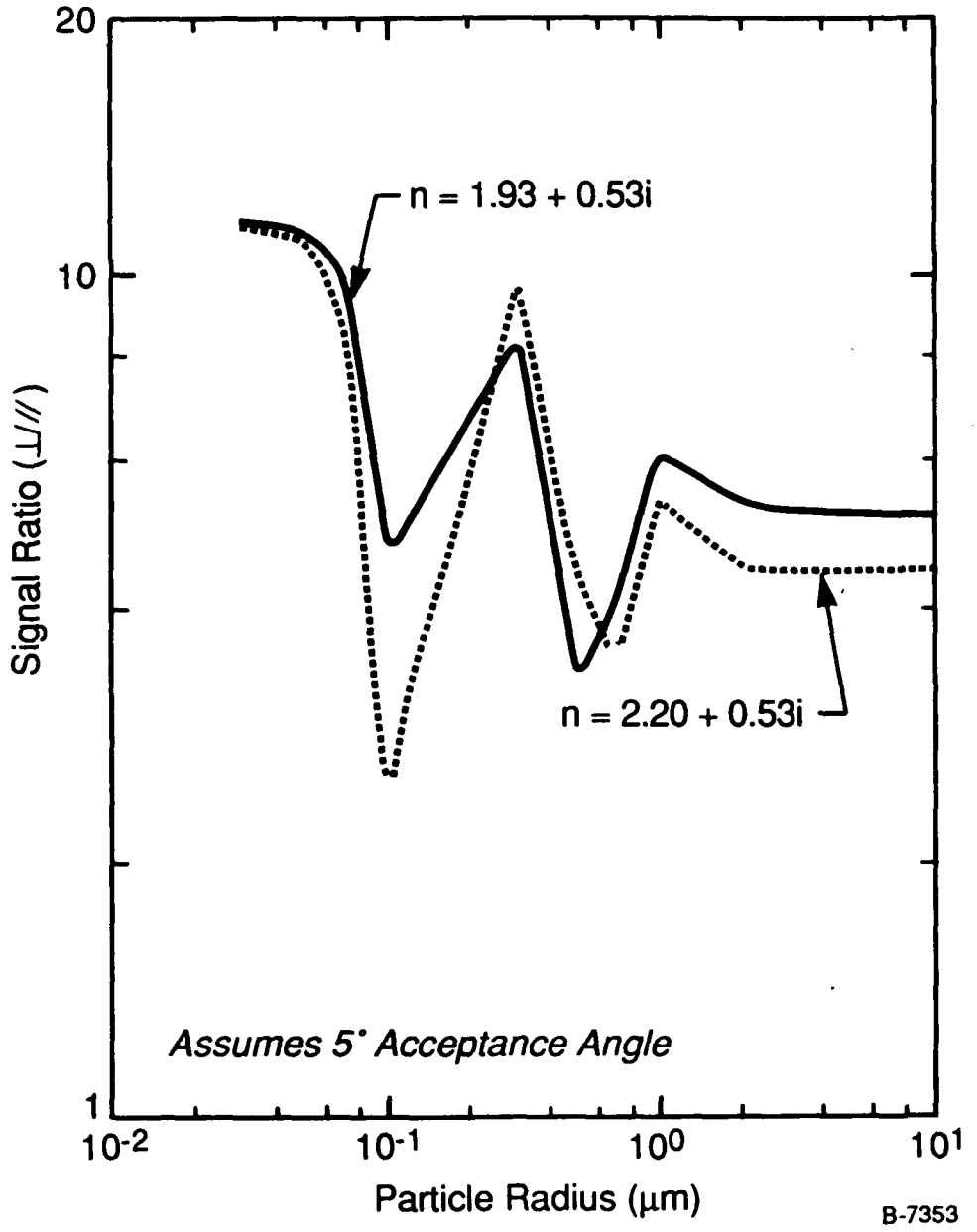

Figure 13. Theoretical Prediction of the Scattering Cross Section Ratio at 90 Deg Between Perpendicular and Parallel Polarized Light at 514.5 nm. The prediction includes an assumed 5 deg uncertainty in the polarization ratio

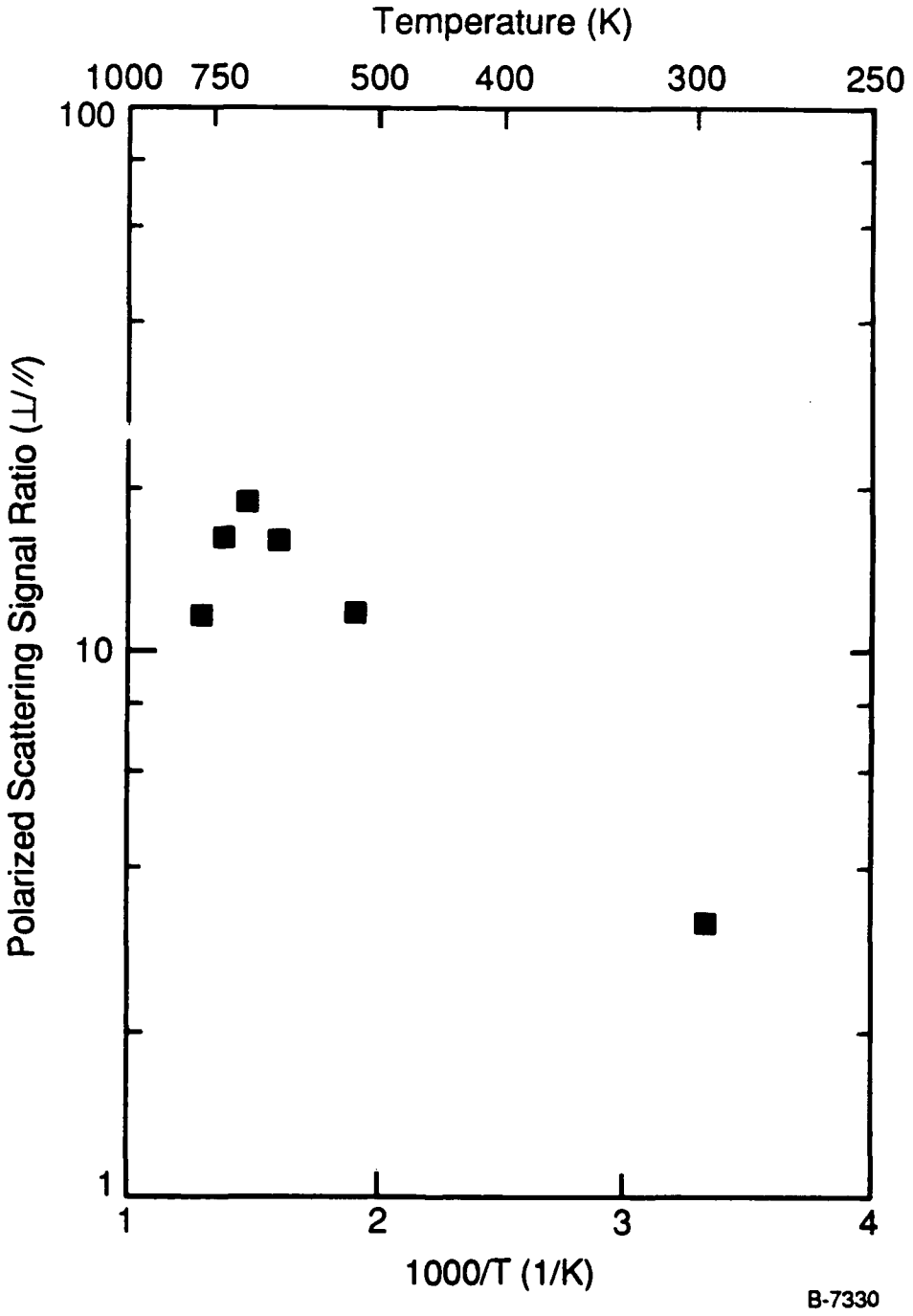

Figure 14. Observed Signal Ratios for Scattering at 90 Deg for Perpendicular to Parallel Polarization States

The fluorescence signal generated by the 514.5 nm laser was monitored concurrently with the scattering signal and the results are shown in Figure 15. Both the scattering and fluorescence signal required correction for optical absorption and the interpolated/extrapolated results for both 500 and 525 nm were used to define the correction. Fluorescence signals included as part of Figure 15 are the signal intensities using a long-pass 550 nm blocking filter to remove scattered light from the laser. Results for both scattering and fluorescence follow a dual slope behavior with a shallow slope at the lower temperatures and a steep slope at the higher temperatures. The transition temperature is approximately 630 K. The scattering signal will be uniquely related to particulate since the scattering signal is generated by the interaction of the probe laser with particles. Fluorescence, however, may be generated by either the interaction of the laser with particulate or molecular species. It is interesting to note that the fluorescence and scattering signal follow the same general behavior indicating that fluorescence and scattering are either following the same species (particulate) or species that change with temperature in a similar fashion. Differences in the relative scattering to fluorescence data could either be due to the change in particle size (fluorescence is fundamentally an absorption process; absorption cross section is a function of r^3 and scattering is a function of r^6) or to the changes in the relative concentration of molecular and particulate fluorescing species.

As a means of further examining the fluorescence data, a series of fluorescence measurements was performed using progressively longer wavelength filters. The filter transmission curves are shown in Figure 16 and a coarse fluorescence spectrum may be constructed using results from these filters. Signal differences between adjacent wavelengths may be constructed to include only the signal for the region between two filters; as an example the signal from 590 nm subtracted from the 570 nm signal includes only signal of fluorescence between 570 and 590 nm. Relative fluorescence spectra can therefore be computed by differencing the signal levels and adjusting the derived signals for effective optical bandwidth and relative photomultiplier tube response. Results are shown in Figures 17 and 18.

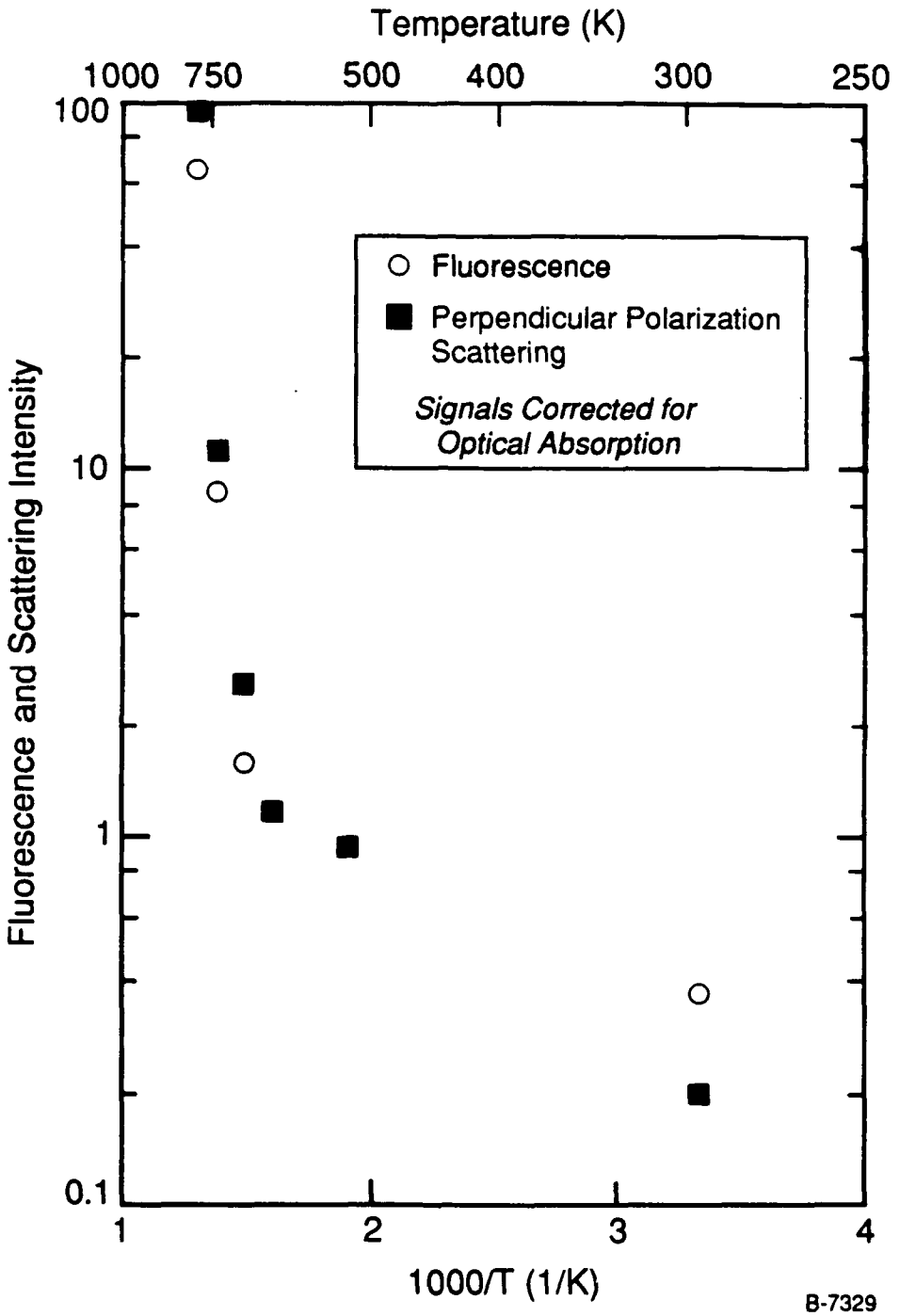

Figure 15. Fluorescence and Scattering Intensity as a Function of Temperature for JP-4. Both results have been corrected for optical absorption. Probe wavelength is 514.5 and fluorescence is from wavelengths larger than 550 nm

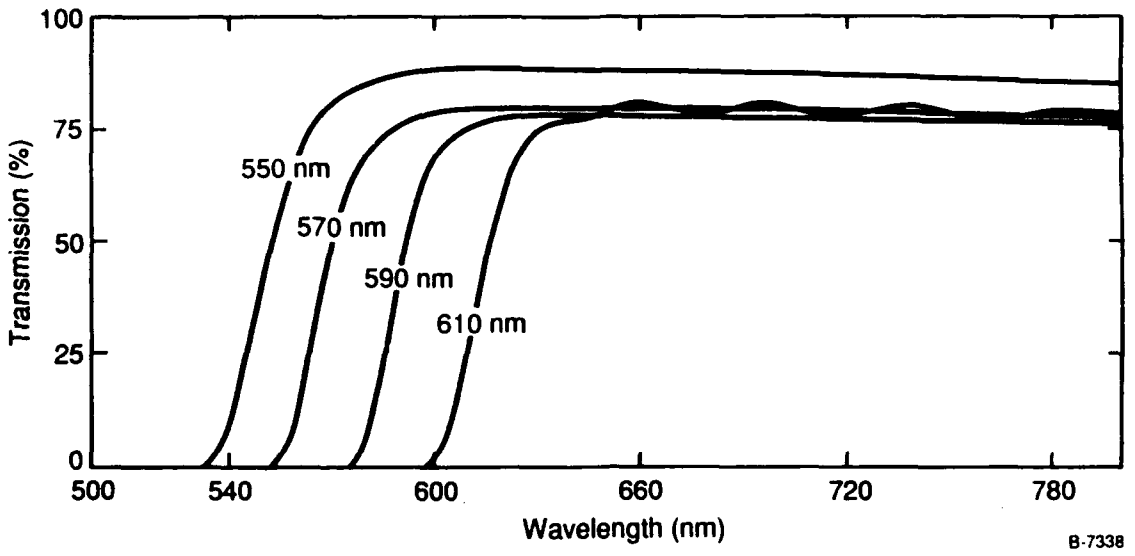

Figure 16. Filter Transmission Curves for the Successive Filters Used to Monitor Fluorescence from JP-4

Figure 17 illustrates the fluorescence spectra for room temperature fuel and fuel that has been processed at 526 and 625 K. Each of these spectra is different which indicates that the combination of fluorescing species is different. Figure 18 illustrates the high temperature fluorescence results. These spectra are much more similar to each other implying that for high temperatures, the fluorescence signal may be due to the same species. Clearly the fluorescence spectra would benefit from a higher wavelength resolution such as that afforded by an Optical Multichannel Analyzer (OMA) and the use of fluorescence as a monitor of fuel fouling processes requires further development. However, the simplicity of fluorescence measurements in addition to the possibility of differentiating between fluoresing species by examining the spectra makes it a potentially powerful tool.

5. CONCLUSIONS

The purpose for this work was to examine a variety of optical measurement techniques and their applicability to the fuel fouling problem. All of the measurements were taken using a constant surface heated tube which fed into an optical cell. This apparatus

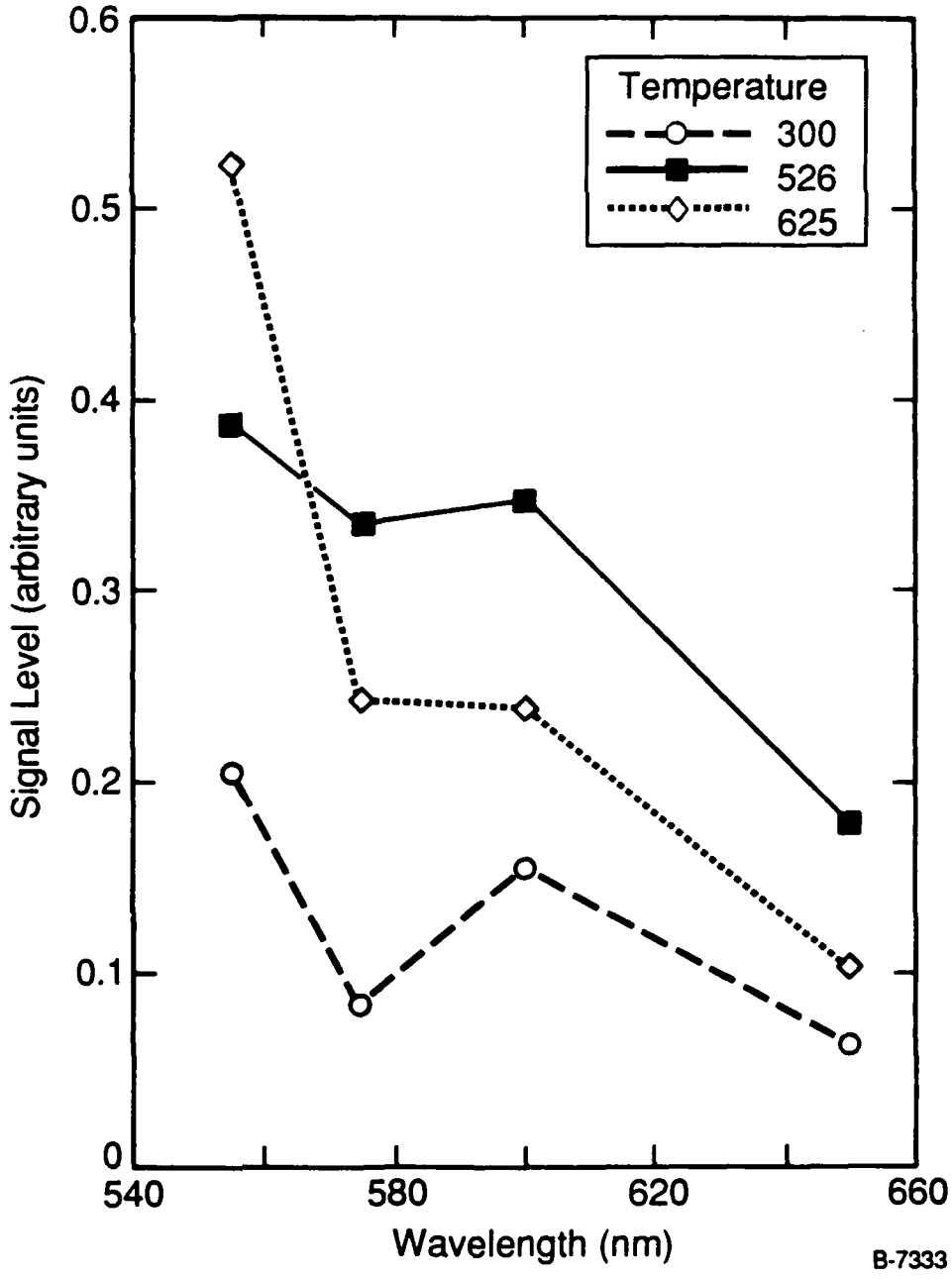

Figure 17. Fluorescence Spectrum for Fuel at Low Temperatures

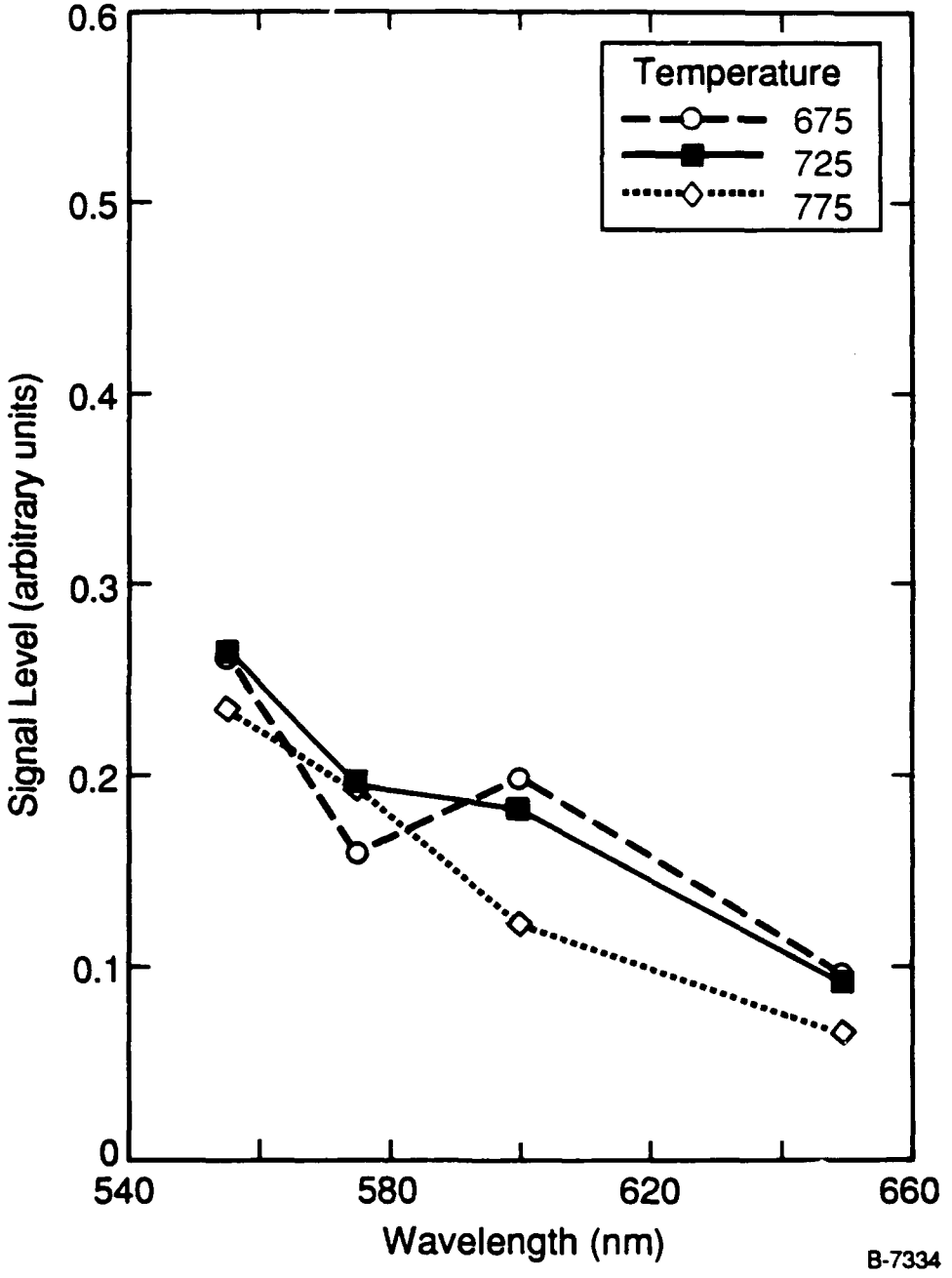

Figure 18. Fluorescence Spectrum for Fuel at High Temperatures

provided a stable and carefully controlled environment for studying fuel fouling. Absorption measurements for 375 to 750 nm at temperatures between ambient and 680 K and pressure equal to 400 psig, indicated dramatic changes in the thermally stressed fuel. These changes included indications of both molecular changes in the fuel composition and a dramatic increase in the particulate present in the flow. Comparative kinetic results demonstrate the primary importance of temperature in controlling these changes, with a secondary dependence on residence time. The relative kinetic behavior for the absorption measurement could also be grouped into a low and high temperature regime which displayed a constant slope behavior in an Arrhenius format. The transition temperature between these two regions was observed to be approximately 525 K. Scattering sizing measurements were also performed for room temperature and thermally stressed fuel. This measurement was used to identify the size class of particulate present in the system. Room temperature fuel was observed to contain particulate with radii greater than 0.1 μm, while the results for fuel between 500 and 800 K indicated radii of less than 0.06 μm. Observed fluorescence signals were very strong with a varying spectral structure over the room to high temperature range. In addition the general behavior of scattering and fluorescence signals was very similar which indicates that the two measurements monitor either the same species or species with similar temperature behavior.

The absorption, scattering, and fluorescence all displayed an ability to monitor changes within the thermally stressed fuel. However, the fuel fouling problem is exceptionally complex and no single measurement, at this time, is appropriate for monitoring all processes within the fuel. Our recommendation, based upon the promising results contained within this paper, is to continue to attack the fuel fouling problem with a multitude of optical measurement techniques that are coupled to more classical evaluation methods such as post-thermal stress, chemical analysis, and carbon deposition rate studies. The combination of the classical and optical techniques will produce both a new understanding of the processes involved in fuel fouling and possibly produce new methods for evaluating the thermal stability of fuels.

6. REFERENCES

1. Roquemore, W.M., Pearce, J.A., Harrison, W.E., Krazinski, J.L., and Vanka, S.P., "Fouling in Jet Fuels: New Approach," presented at 198th National ACS Meeting, Miami Beach, Florida, September 1989.

2. Johnson, J., Chiantelb, A.J., and Cashost, H.W., "Application of Light Scattering to Diesel Fuel Stability Problems," Ind. and Eng. Chem. 47(6), 1226-1230 (1955).

3. Taylor, W.F. and Wallace, T.J., "Kinetics of Deposit Formation from Hydrocarbon Fuels at High Temperatures," I and EC Prod. Res. and Devel. 6(4), 258-762 (1967).

4. Taylor, W.F. and Wallace, T.J., "Kinetics of Deposit Formation from Hydrocarbons: Effects of Trace Sulfur Compounds," I and EC Prod. Res. and Devel. 7(3), 198-702 (1968).

5. Taylor, W.F., "Kinetics of Deposit Formation from Hydrocarbons," I and EC Prod. Res. and Devel., 375-380 (1969).

6. Taylor, W.F., "Deposit Formation from Deoxygenated Hydrocarbons: I. General Features," Ind. and Eng. Chem. Prod. Res. and Devel. 13(2), 133-138 (1974).

7. Taylor, W.F., "Deposit Formation from Deoxygenated Hydrocarbons: II. Effect of Trace Sulfur Compounds," Ind. and Eng. Chem. Prod. Res. and Devel. 15(1), 64-68 (1976).

8. Szeta, E.J., Giovanetti, A.J., and Cohen, S., "Fuel Deposit Characteristics of Low Velocity," Transcript of the ASME 108, 460-464 (1986).

9. Kendall, D.R. and Mills, S.S., "Thermal Stability of Aviation Kerosines: Techniques to Characterize Their Oxidation Properties," Ind. and Eng. Chem. Prod. Res. and Devel. 75(2), 360-365 (1986).

10. Mills, S.S. and Kendall, D.R., "The Quantification and Improvement of the Thermal Stability of Aviation Turbine Fuel," Journal of Engineering for Gas Turbines and Power 108, 381-386 (1986).

11. Kays, W.M. and Crawford, M.F., Convective Heat and Mass Transfer, McGraw-Hill Book Co., New York (1980).

12. Melles Griot Optics Guide 3, Melles Griot, Irvine, CA, 55-56 (1985).

13. Weast, R.C., Handbook of Chemistry and Physics (50th Edition), Chemical Rubber Co., Cleveland, OH (1970).

14. Herzberg, G., Molecular Spectra and Molecular Structure: III. Electronic Spectra and Electronic Structure of Polyatomic Molecules, Van Nostrand Reinhold Co., New York (1966).

15. Friedel, R.A. and Orchin, M., Ultraviolet Spectra of Aromatic Compounds, John Wiley and Sons, Inc., New York (1951).

16. Hana, M.W., Quantum Mechanics in Chemistry, W.A., Benjamin Inc., Menlo Park, CA (1969).

17. van de Hulst, H.C., Light Scattering by Small Particles, Dover Publications, Inc., New York (1981).

18. Lee, S.C. and Tien, C.L., "Optical Constants of Soot in Hydrocarbon Flames," 18th Symposium (Int'l) on Combustion, 1159-1166 (1981).

19. Bohren, C.F. and Huffman, D.R., Absorption and Scattering of Light by Small Particles, John Wiley and Sons (1983).

APPENDIX A

This appendix contains the spectrally resolved absorption data. The figures show absorption as a function of wavelength for thermally stressed JP-4.

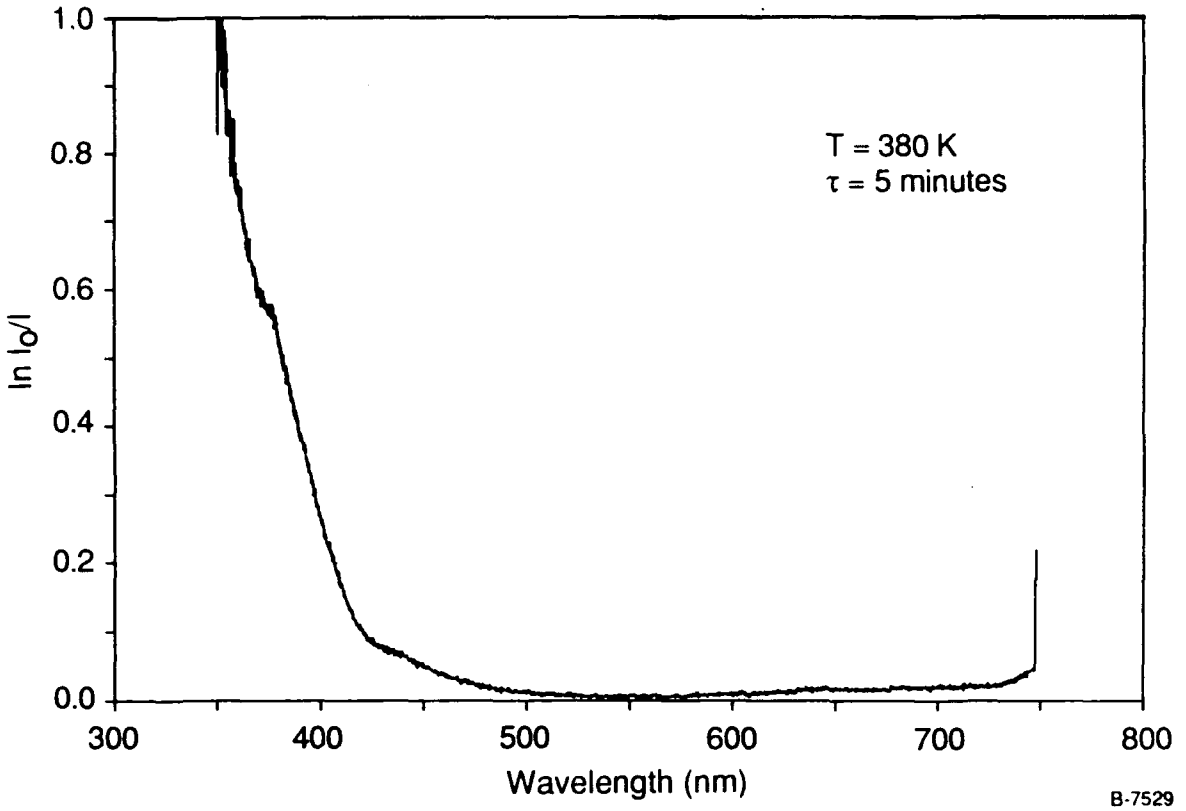
T = 380 K
τ = 5 minutes
ln I_O/I
1.0
0.8
0.6
0.4
0.2
0.0
300
400
500
600
700
800
Wavelength (nm)
B-7529

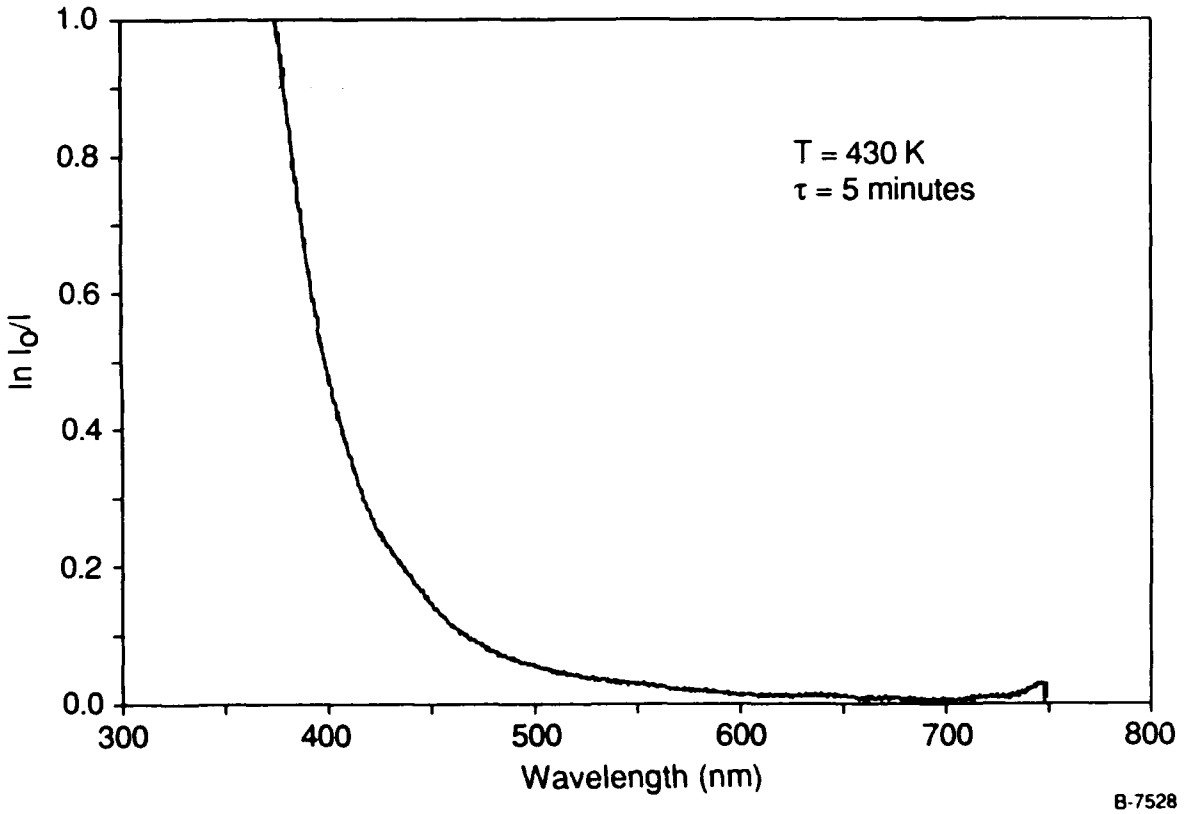
T = 430 K
τ = 5 minutes
ln I_O/I
1.0
0.8
0.6
0.4
0.2
0.0
300
400
500
600
700
800
Wavelength (nm)
B-7528

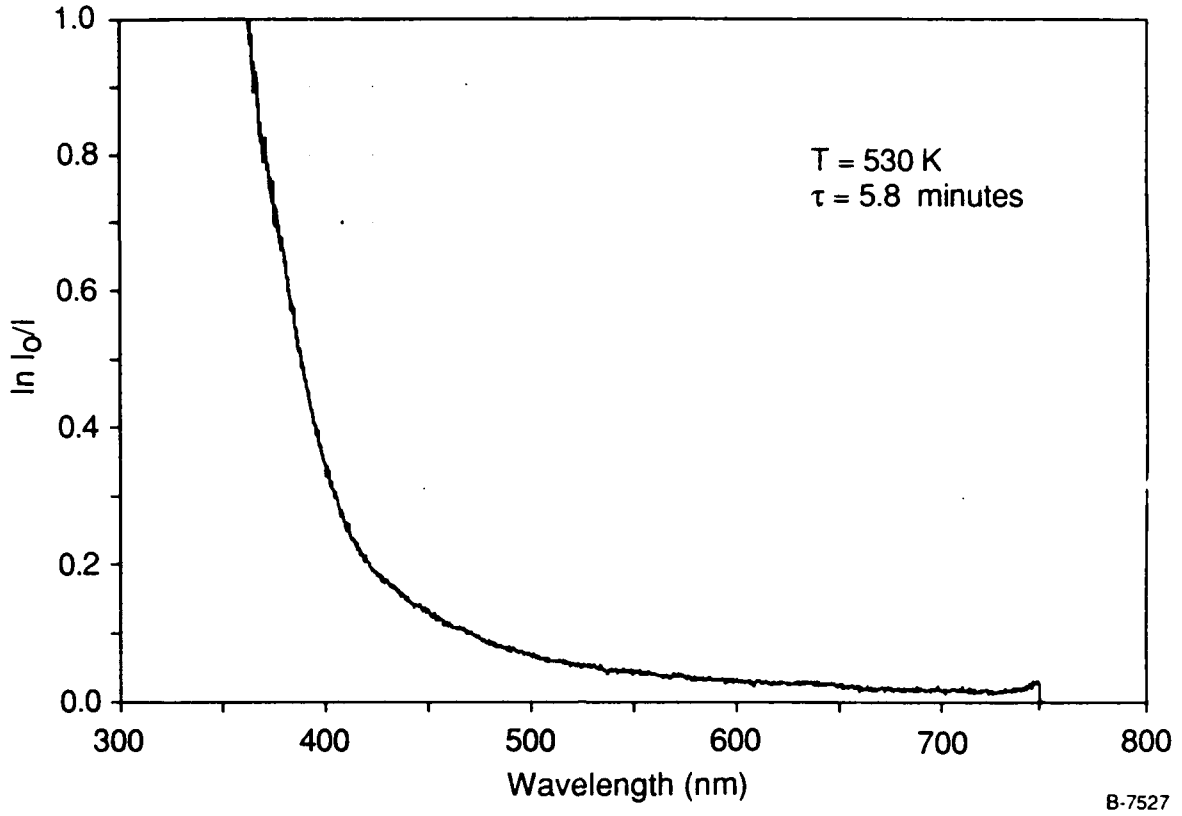
1.0
0.8
0.6
0.4
0.2
0.0
ln I_O/I
T = 530 K
τ = 5.8 minutes
300
400
500
600
700
800
Wavelength (nm)
B-7527

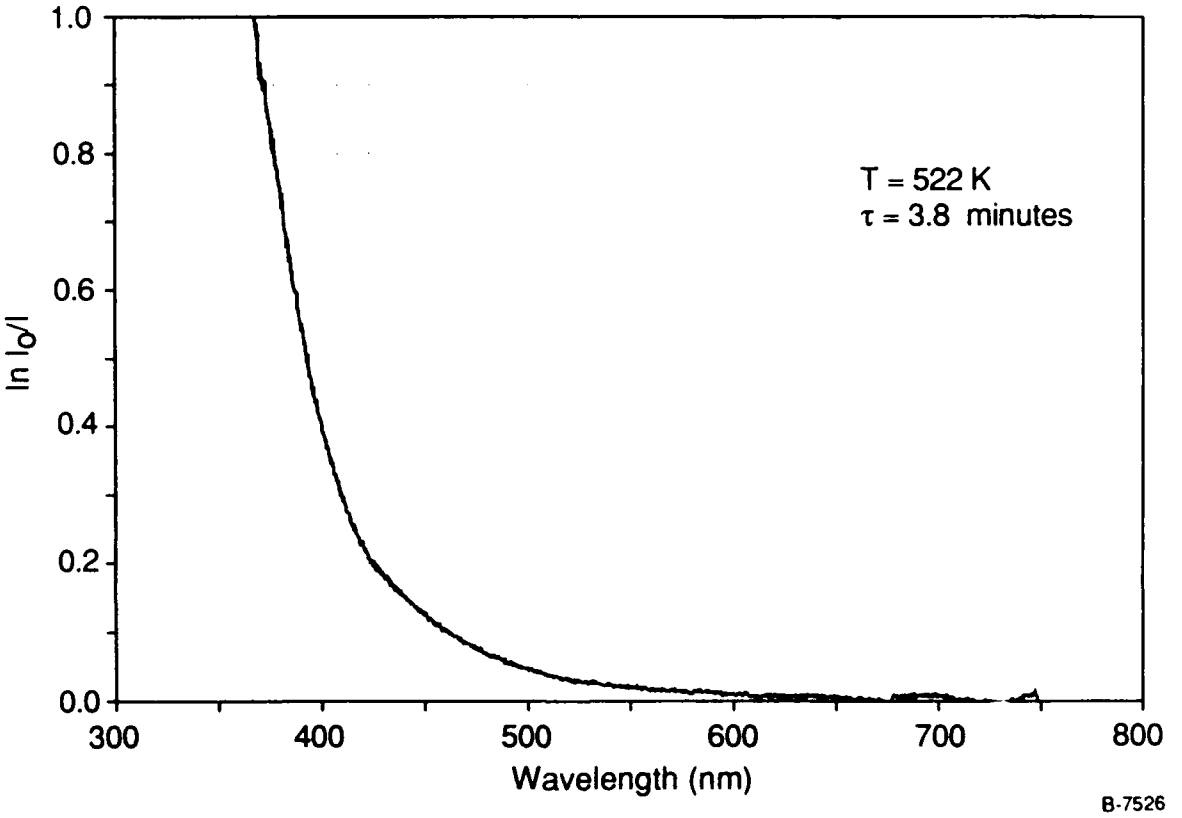
1.0
0.8
0.6
0.4
0.2
0.0
ln I_O/I
T = 522 K
τ = 3.8 minutes
300
400
500
600
700
800
Wavelength (nm)
B-7526

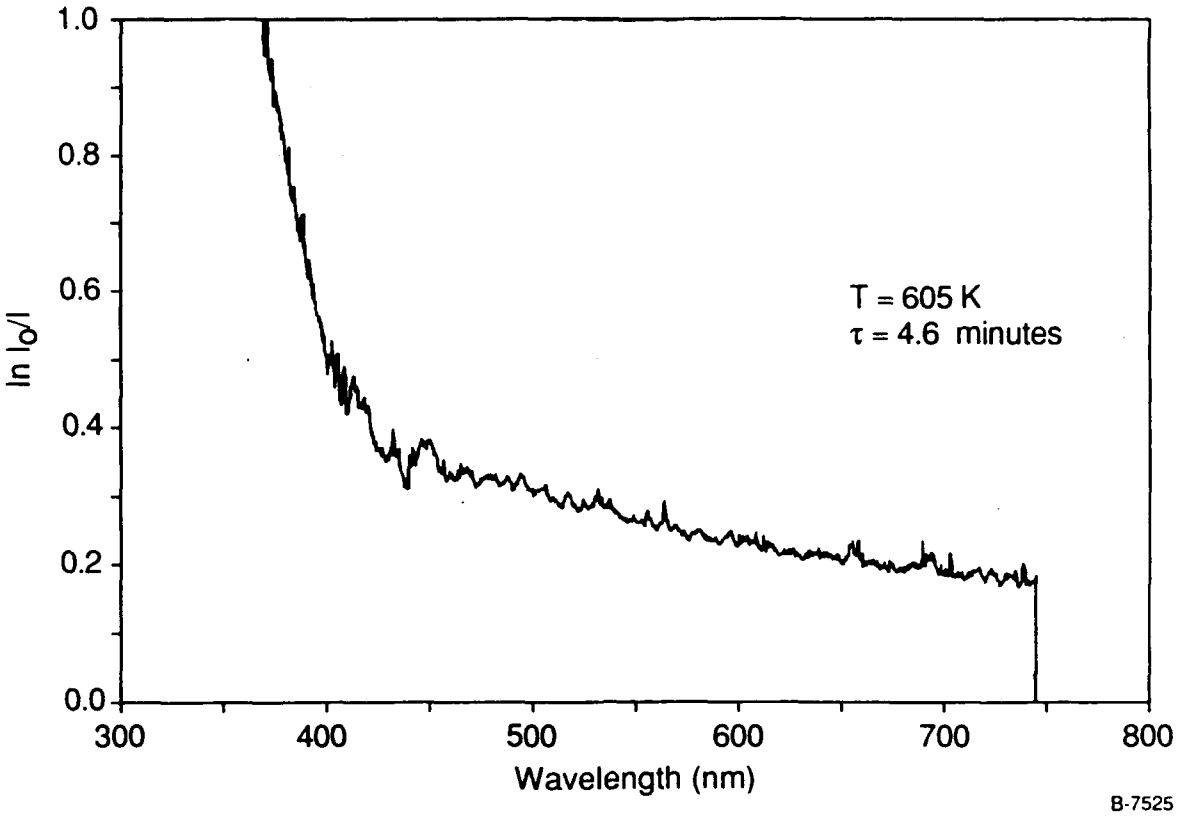
1.0
0.8
0.6
0.4
0.2
0.0
ln I_0/I
T = 605 K
τ = 4.6 minutes
300
400
500
600
700
800
Wavelength (nm)
B-7525

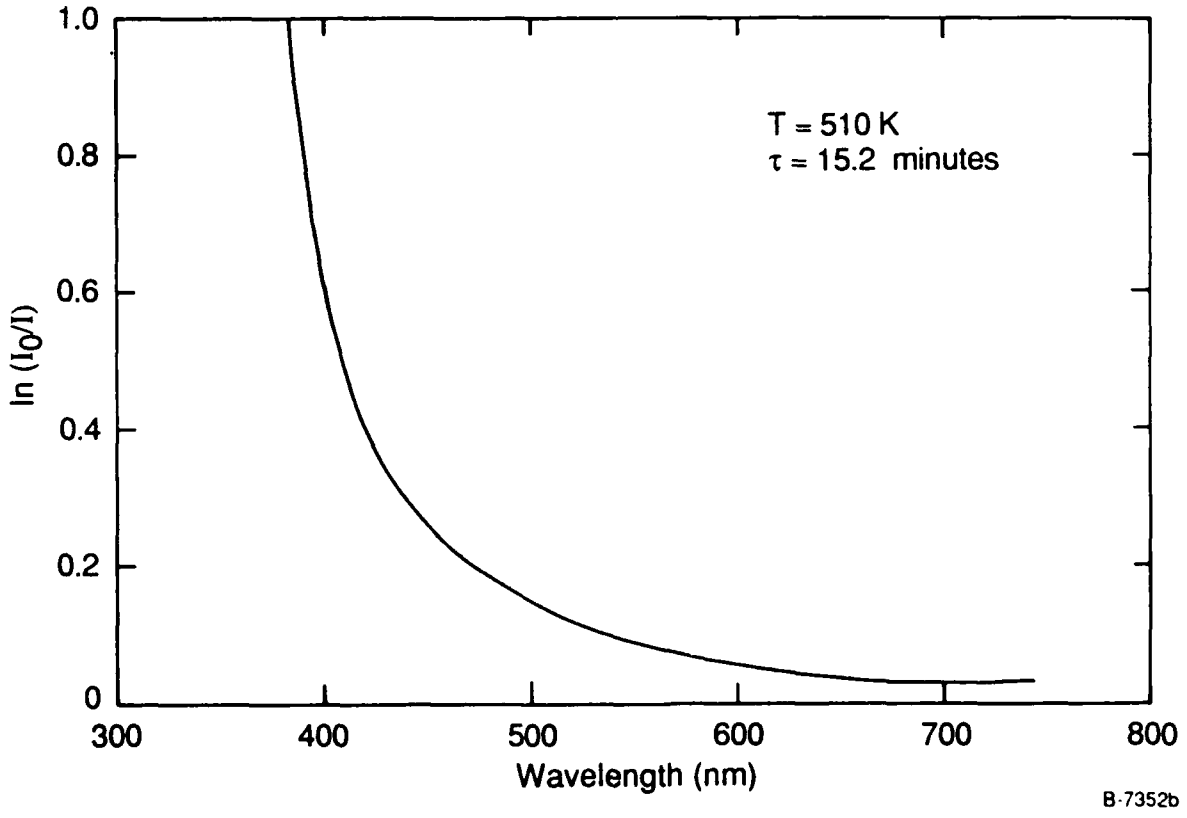
1.0
0.8
0.6
0.4
0.2
0
ln (I_0/I)
T = 510 K
τ = 15.2 minutes
300
400
500
600
700
800
Wavelength (nm)
B-7352b

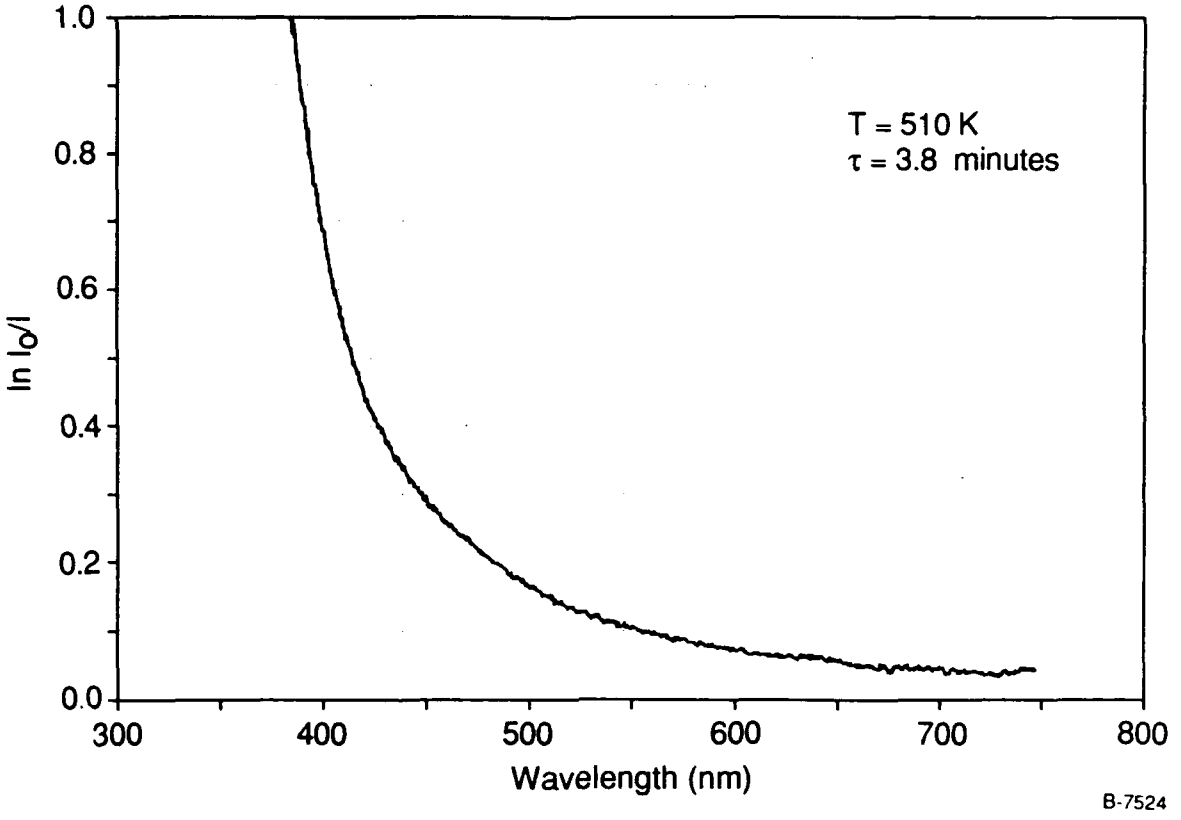
T = 510 K
τ = 3.8 minutes
ln I0/I
1.0
0.8
0.6
0.4
0.2
0.0
300
400
500
600
700
800
Wavelength (nm)
B-7524

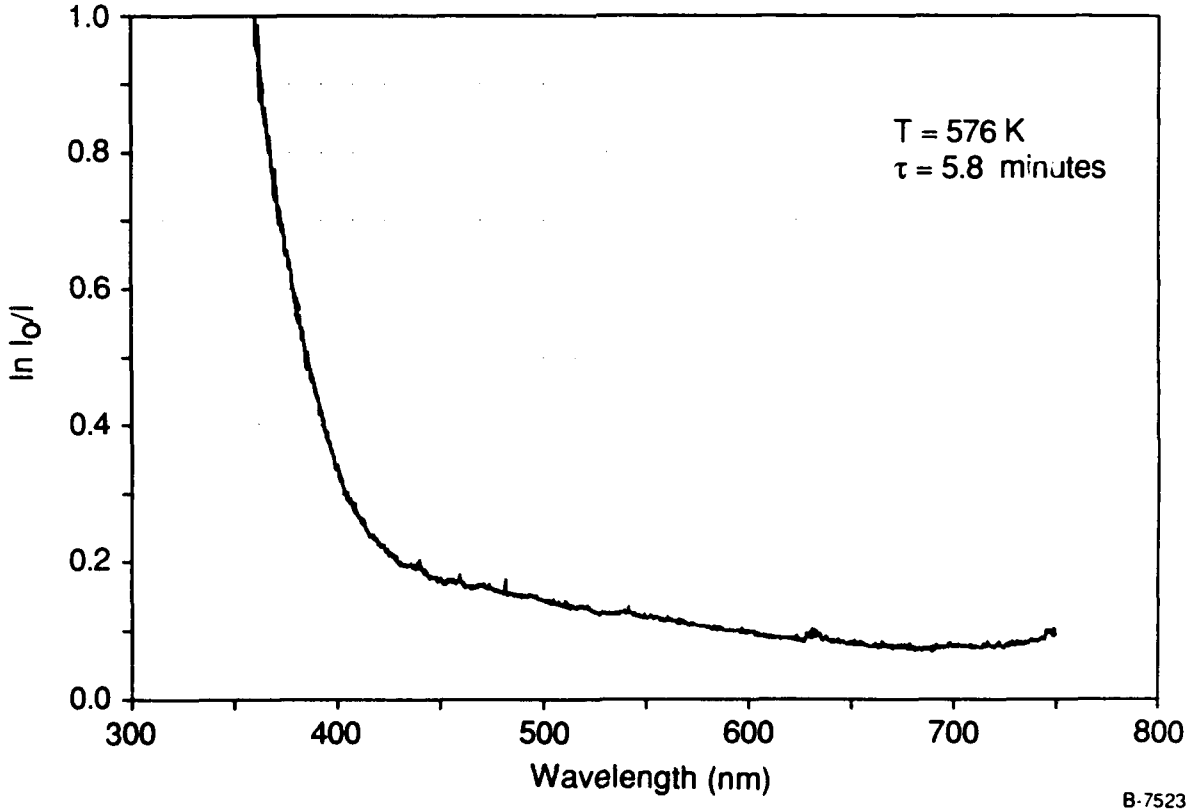
T = 576 K
τ = 5.8 minutes
ln I0/I
1.0
0.8
0.6
0.4
0.2
0.0
300
400
500
600
700
800
Wavelength (nm)
B-7523

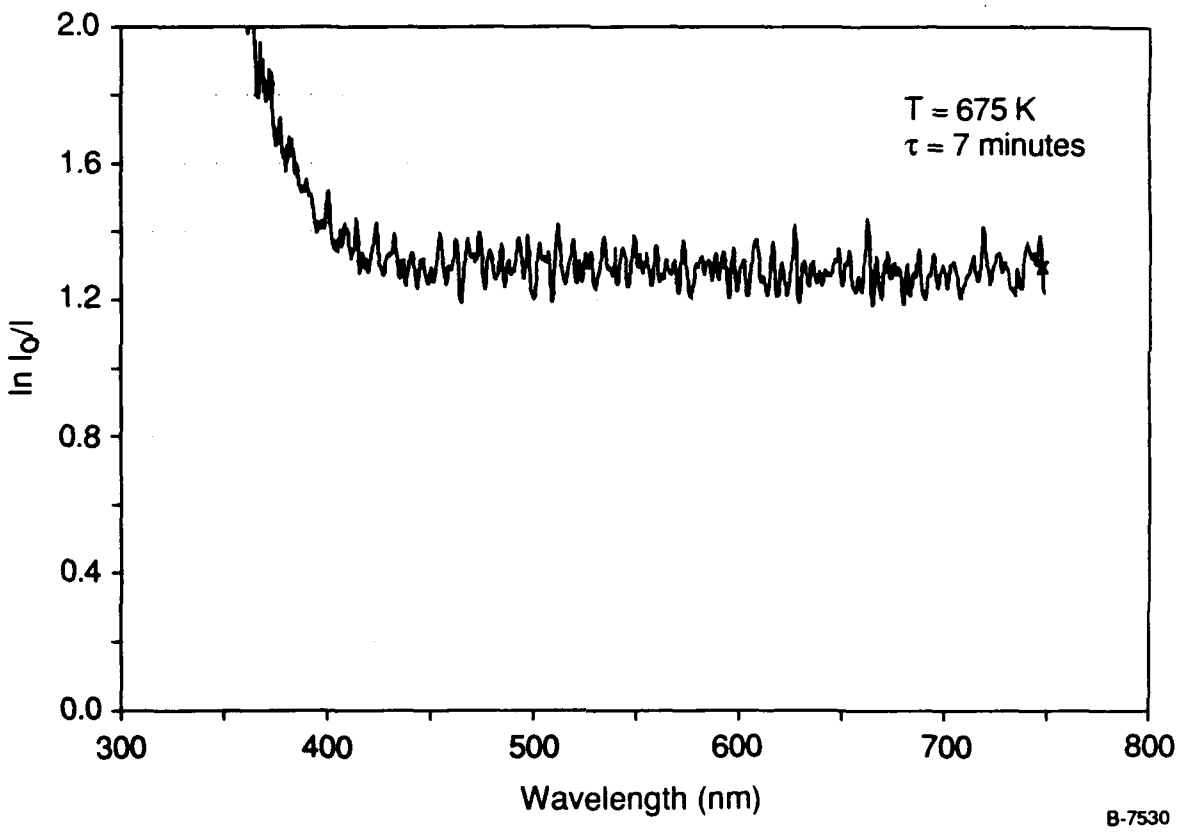
2.0
1.6
1.2
0.8
0.4
0.0
ln I_0/I
T = 675 K
τ = 7 minutes
300
400
500
600
700
800
Wavelength (nm)
B-7530

APPENDIX B

This appendix contains transmission covers for JP-4 which has been thermally stressed, re-collected, and analyzed with a spectrophotometer. Samples were held in a Quartz cell with a 10 mm path length. Transmission curves for the cell and JP-4 in its as-received condition are also included.

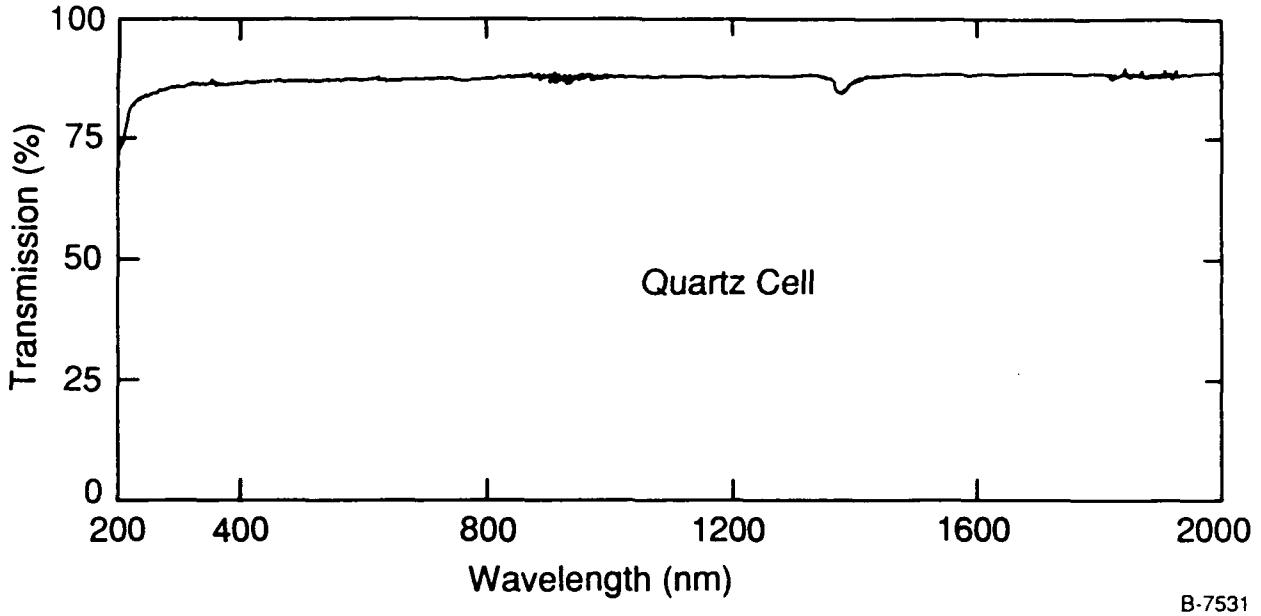
100
75
50
25
0
Transmission (%)
Quartz Cell
200
400
800
1200
1600
2000
Wavelength (nm)
B-7531

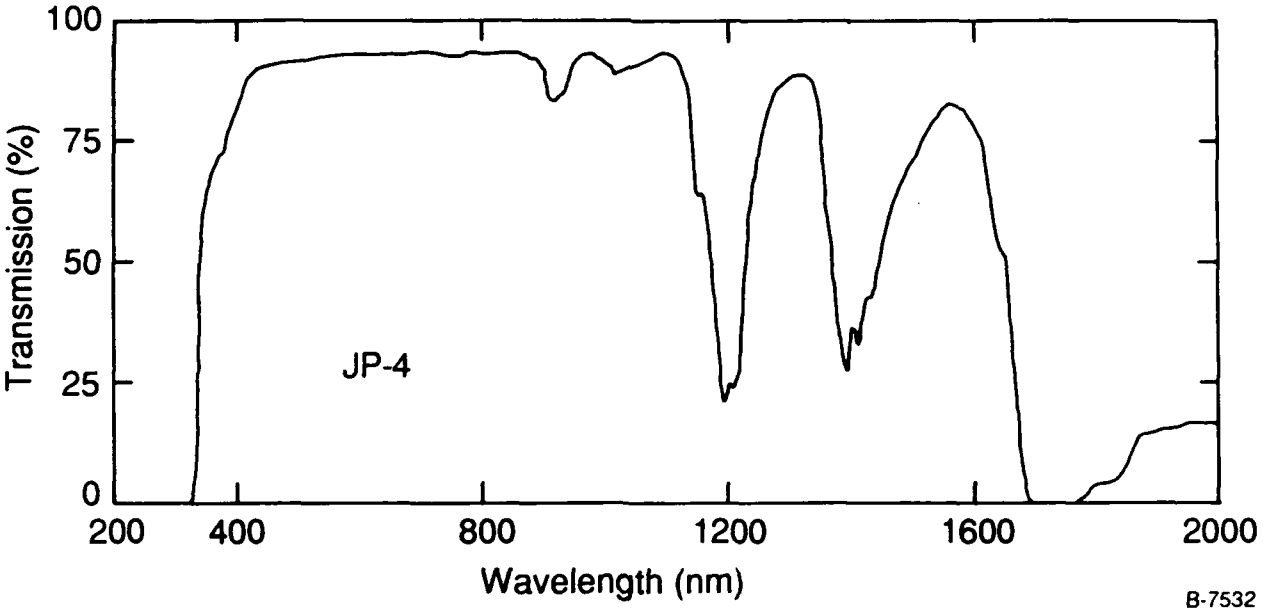
100
75
50
25
0
Transmission (%)
JP-4
200
400
800
1200
1600
2000
Wavelength (nm)
B-7532

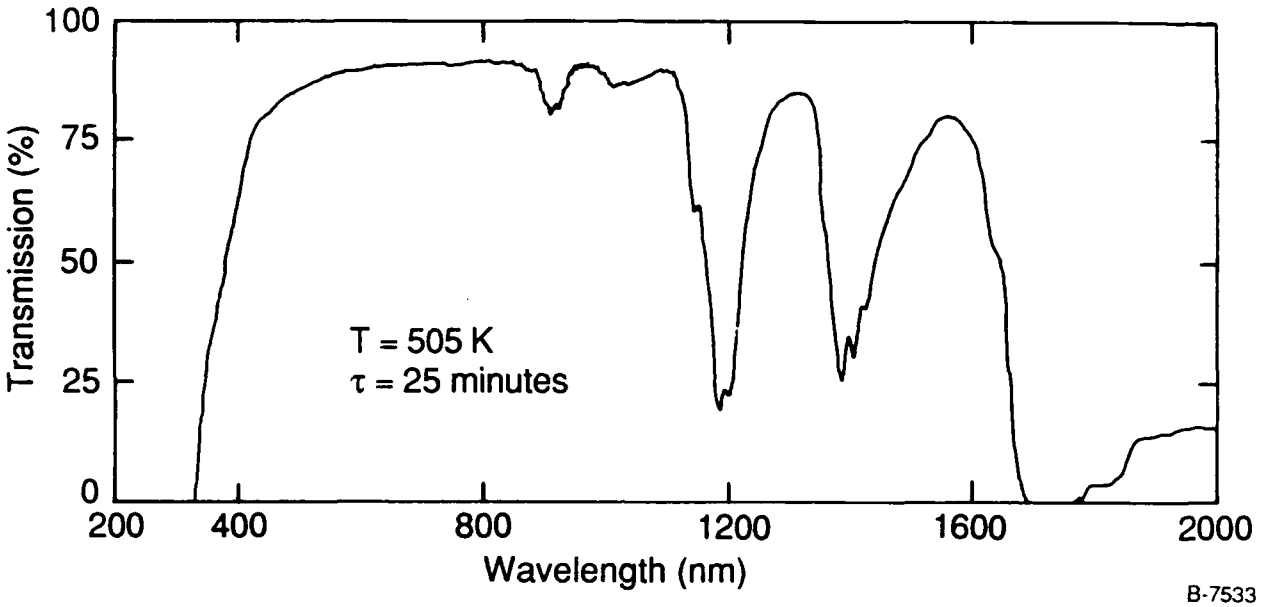
100
75
50
25
0
Transmission (%)
T = 505 K
τ = 25 minutes
200
400
800
1200
1600
2000
Wavelength (nm)

B-7533

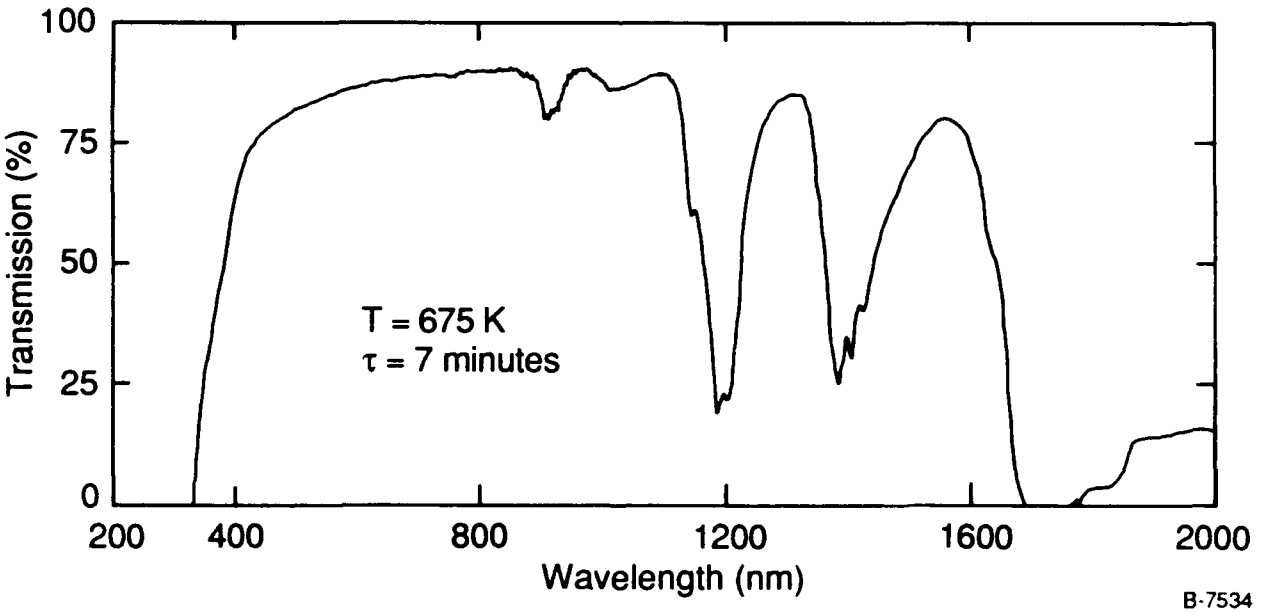
100
75
50
25
0
Transmission (%)
T = 675 K
τ = 7 minutes
200
400
800
1200
1600
2000
Wavelength (nm)

B-7534